Identification of a Non-Growth Factor Role for GM-CSF in Advanced Atherosclerosis
Promotion of Macrophage Apoptosis and Plaque Necrosis Through IL-23 Signaling

Manikandan Subramanian, Edward Thorp, Ira Tabas

Rationale: Granulocyte macrophage colony-stimulating factor (GM-CSF, Csf2) is a growth factor for myeloid-lineage cells that has been implicated in the pathogenesis of atherosclerosis and other chronic inflammatory diseases. However, the role of GM-CSF in advanced atherosclerotic plaque progression, the process that gives rise to clinically dangerous plaques, is unknown.

Objective: To understand the role of GM-CSF in advanced atherosclerotic plaque progression.

Methods and Results: $Ldlr^{-/-}$ mice and $Csf2^{-/-}Ldlr^{-/-}$ mice were fed a Western-type diet for 12 weeks, and then parameters of advanced plaque progression in the aortic root were quantified. Lesions from the GM-CSF–deficient mice showed a substantial decrease in 2 key hallmarks of advanced atherosclerosis, lesional macrophage apoptosis and plaque necrosis, which indicates that GM-CSF promotes plaque progression. Based on a combination of in vitro and in vivo studies, we show that the mechanism involves GM-CSF–mediated production of interleukin-23, which increases apoptosis susceptibility in macrophages by promoting proteasomal degradation of the cell survival protein Bcl-2 (B-cell lymphoma 2) and by increasing oxidative stress.

Conclusions: In low-density lipoprotein–driven atherosclerosis in mice, GM-CSF promotes advanced plaque progression by increasing macrophage apoptosis susceptibility. This action of GM-CSF is mediated by its interleukin-23–inducing activity rather than its role as a growth factor. (*Circ Res*. 2015;116:e13-e24. DOI: 10.1161/CIRCRESAHA.116.304794.)

Key Words: apoptosis ∎ atherosclerosis ∎ cytokines ∎ granulocyte macrophage colony-stimulating factor ∎ intercellular signaling peptides and proteins ∎ interleukin-23

Granulocyte macrophage colony-stimulating factor (GM-CSF) is generally considered a hematopoietic growth factor with particular roles in myeloid cell development and mice lacking GM-CSF or its receptor have deficits in specific populations of nonlymphoid tissue resident dendritic cells (DCs) under homeostatic conditions.[1] However, these mice have normal levels of myeloid immune cell populations in the peripheral circulation and lymphoid organs.[1] Thus, it is important to consider other roles for GM-CSF in physiological and pathophysiologic settings, such as its ability to promote cytokine production. For example, GM-CSF primes macrophages for the production of proinflammatory cytokines after exposure to lipopolysaccharide or tumor necrosis factor-α[2] and induces interleukin (IL)-23 production in DCs and macrophages.[3,4]

Editorial, see p 222

Understanding the role of GM-CSF in atherosclerosis, particularly its effect on the types of necrotic plaques that give rise to acute atherothrombotic disease in humans, is important for several reasons. First, atherosclerosis is driven by a variety of lesional myeloid cell processes,[5] suggesting a potentially important role for this myeloid cell-relevant protein. Second, GM-CSF production by cultured macrophages is induced by incubation with atherogenic lipoproteins,[6] and GM-CSF is expressed in murine and human atherosclerotic lesions.[7,8] Third, in a small study in which GM-CSF was administered to patients with stable coronary artery disease to improve collateral artery formation, several of the subjects experienced acute coronary events.[9] In this context, in a preclinical study of GM-CSF therapy for atherosclerosis in rabbits, there were features suggesting accelerated advanced plaque progression despite a decrease in overall intimal area.[10] Fourth, GM-CSF is administered to patients with cancer after chemotherapy to mobilize

DOI: 10.1161/CIRCRESAHA.116.304794

Nonstandard Abbreviations and Acronyms	
7KC	7-ketocholesterol
DC	dendritic cell
GM-CSF	granulocyte macrophage colony-stimulating factor
IL	interleukin
ROS	reactive oxygen species
TUNEL	terminal deoxynucleotidyl transferase dUTP nick end labeling
WD	Western-type diet

stem cells,[11] whereas anti–GM-CSF therapy is under trial for the treatment of rheumatoid arthritis and multiple sclerosis.[12] Because these treatments are offered to patients who may have subclinical coronary artery disease, it is important to understand the role of GM-CSF in advanced plaque progression.

In theory, both growth factor and non–growth factor roles of GM-CSF could be important in atherosclerosis. In animal models of atherosclerosis, the effects of GM-CSF deficiency or exogenous GM-CSF administration on atherosclerosis have been variable and dependent on the specific animal model tested.[7,10,13,14] However, most of these studies used models and reported end points most relevant to early atherogenesis, such as lesion size and cellularity, not advanced plaque progression. In this regard, most clinically relevant plaques in humans are distinguished not by their large size and cellularity but rather by features of plaque instability, notably plaque necrosis.[15] A major cause of advanced plaque necrosis is accelerated lesional macrophage apoptosis coupled with defective efferocytic clearance of the dead cells, leading to postapoptotic necrosis and necrotic core formation.[16] Advanced plaques are also characterized by excessive oxidative stress, which promotes macrophage apoptosis.[17,18]

To address this gap, we conducted a study in *Csf2$^{-/-}$Ldlr$^{-/-}$* mice subjected to prolonged Western-type diet (WD) feeding and focused on lesional cell apoptosis and necrotic core formation. We observed that the aortic root lesions of these GM-CSF–deficient mice had a substantial decrease in apoptotic cells, plaque necrosis, and oxidative stress compared with lesions of control *Ldlr$^{-/-}$* mice. The mechanism involves GM-CSF–mediated induction of IL-23 in myeloid cells, which then sensitizes macrophages to apoptosis via proteasomal degradation of Bcl-2. The decrease in Bcl-2 increases caspase-9 activation and promotes proapoptotic oxidative stress. Thus, a non–growth factor function of GM-CSF promotes advanced plaque progression through an IL-23–mediated signaling pathway in macrophages that increases their susceptibility to apoptosis. These findings reveal a new pathway that contributes to advanced lesional macrophage apoptosis, which may be relevant to contemplated or actual situations where GM-CSF or IL-23 is used as a treatment modality in humans.

Methods

Animals and Animal Maintenance

Csf2$^{-/-}$ mice on a C57BL/6J background were generously provided by Dr Bruce Trapnell (University of Cincinnati College of Medicine). *Csf2$^{-/-}$* mice were bred with C57BL/6J *Ldlr$^{-/-}$* mice (Jackson laboratories) to generate *Csf2$^{-/-}$Ldlr$^{-/-}$* mice. Six-week-old *Ldlr$^{-/-}$* or *Csf2$^{-/-}$Ldlr$^{-/-}$* mice were fed a WD (Harlan Teklad, TD88137) ad libitum for 12 weeks to generate advanced atherosclerotic lesions. All protocols were approved by the Columbia University Institutional Animal Care and Use Committee (IACUC).

Atherosclerotic Lesion Analysis and Metabolic Profiling

Animals were euthanized at the end of the WD feeding period using isoflurane inhalation, and blood was withdrawn by cardiac puncture. The heart with the aortic root attached was harvested, embedded in optimum cutting temperature and frozen on dry ice. Aortic root sections were prepared using a cryomicrotome and then stained with hematoxylin and eosin. Six sections per mouse were quantified for total lesion area and necrotic area as described previously.[19] Briefly, the intimal region containing lesions is demarcated and quantified using ImagePro Plus by a person blinded to the experimental groups. Similarly, the necrotic area is marked and quantified as an area of the lesion that is devoid of cellular nuclei. Plasma cholesterol and triglycerides were measured using the Cholesterol E kit and Triglyceride M Color B kit from Wako. Fasting blood glucose was measured using glucose test strips and a glucometer. Plasma insulin was analyzed using an insulin ELISA kit (Crystal Chem).

Apoptosis and In Situ Efferocytosis Assays

Apoptosis in cultured macrophages was assayed using Alexa Fluor-conjugated annexin-V labeling (Life Technologies), followed by fluorescence microscopy. A total of 600 cells per group were analyzed to quantify the percentage of cells that were annexin-V positive. Apoptosis in atherosclerotic lesions was detected by terminal deoxynucleotidyl transferase dUTP nick end labeling (TUNEL) staining using the tetramethylrhodamine red in situ cell death detection kit (Roche) following the manufacturer's protocol. The TUNEL-stained sections were analyzed by microscopy and quantification was conducted using ImageJ. Lesional apoptosis was also assayed using activated-caspase-3 immunofluorescence microscopy.[20] In situ efferocytosis quantification was performed as described previously.[21,22] Briefly, aortic root sections were stained with TUNEL followed by anti-F4/80 immunohistochemistry to label lesional macrophages. Efferocytosis efficiency was quantified by counting the number of apoptotic cells that were colocalized or juxtaposed to F4/80-labeled macrophages (associated) versus those that were not associated with macrophages (free).

Statistics

The data are displayed as mean±SEM. The n numbers for each group are indicated in the figure legends. All data presented in this study fit into a normal distribution and hence a Student 2-tailed *t* test was used for determining statistical significance between 2 groups, whereas, a 1-way ANOVA with Bonferroni's correction was applied while evaluating statistical significance between multiple groups. The difference between the mean values was considered significant when the *P* value was <0.05.

Detailed Methods are provided in the Online Data Supplement.

Results

Aortic Root Lesions of WD-Fed *Csf2$^{-/-}$Ldlr$^{-/-}$* Mice Show Decreases in Lesional Cell Apoptosis and Plaque Necrosis

To understand the role of GM-CSF in advanced atherosclerosis, GM-CSF–deficient mice in an atherosclerosis-prone low-density lipoprotein receptor knockout background (*Csf2$^{-/-}$Ldlr$^{-/-}$*) and control *Ldlr$^{-/-}$* mice were fed a WD for 12 weeks. We first confirmed that GM-CSF was absent in the atherosclerotic lesions of *Csf2$^{-/-}$Ldlr$^{-/-}$* mice (Online Figure I). Furthermore, we observed no significant differences between the 2 groups of mice in terms of body weight, total cholesterol, plasma triglycerides, fasting blood glucose, or plasma insulin (Online Table I). When the end point of total aortic root lesional area was assessed, we found that the 2 cohorts were remarkably similar (Figure 1A and 1B), which is largely consistent with a previous study.[13] Also consistent with previous studies,[7,8]
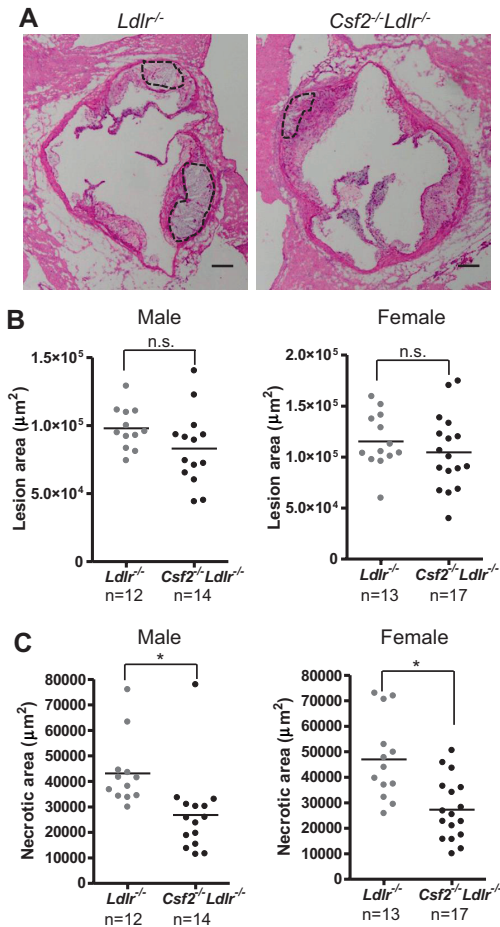
Figure 1. Necrotic area is decreased in the aortic root lesions of granulocyte macrophage colony-stimulating factor (Csf2)–deficient *Ldlr*$^{-/-}$ mice. A, Representative images of hematoxylin–eosin–stained aortic root sections of 12-week Western-type diet–fed *Ldlr*$^{-/-}$ and *Csf2*$^{-/-}$*Ldlr*$^{-/-}$ mice. The necrotic regions are indicated by the broken lines. Bar, 50 μm. **B** and **C**, Measurement of total atherosclerotic lesion area and necrotic area. *$P<0.05$.

we observed that lesional macrophages, DCs, and smooth muscle cells were the major producers of GM-CSF in lesions of *Ldlr*$^{-/-}$ mice (Online Figure II). Because GM-CSF is an important hematopoietic growth factor, we next analyzed the immune cell distribution in the lesions. Overall plaque cellularity was comparable between the 2 groups of mice (Online Figure IIIA). The number of CD11c^{low}F4/80$^+$ cells (macrophages) was not altered by GM-CSF deficiency (Online Figure IIIB). However, as reported in a previous study,[13] we found a modest (≈20%) but statistically significant decrease in the CD11c^{hi}MHCII^{hi} cell population, presumably DCs, in the double knockout plaques (Online Figure IIIB). There was also a decrease in T cells in the *Csf2*$^{-/-}$*Ldlr*$^{-/-}$ lesions (Online Figure IIIB). Note that GM-CSF deficiency was not associated with significant changes in the peripheral blood monocyte or neutrophil count (Online Figure IIIC).

We next examined necrotic area in the lesions because this end point represents a critical advanced lesional characteristic that determines plaque vulnerability in human atherosclerotic lesions.[15] There was an ≈50% decrease in the necrotic area in the GM-CSF–deficient mice (Figure 1A and 1C). Atherosclerotic plaque necrosis is mediated in large part by the combination of lesional cell apoptosis and defective apoptotic cell clearance (efferocytosis).[23] To measure apoptosis, we used the TUNEL staining method and found that the absolute number and percentage of TUNEL-positive lesional cells were significantly lower in the GM-CSF–deficient mice (Figure 2A–2C). The percentage of lesional cells that were positive for cleaved caspase-3, another marker of apoptosis, were also significantly lower in the GM-CSF–deficient mice (Figure 2D; Online Figure IV). This decrease in lesional cell apoptosis in GM-CSF–deficient mice was because of lower numbers and percentages of apoptotic macrophages and DCs, whereas the extent of smooth muscle cell apoptosis was similar between the 2 groups of mice (Online Figure V). Moreover, the ratio of apoptotic cells associated with macrophage phagocytes versus those that were free of phagocytes was similar between the 2 groups of mice (Figure 2E), which indicates that efferocytosis was not affected by GM-CSF deficiency. Two other features of advanced atherosclerosis thinning of the fibrous cap and decreased intimal elastin content were not affected by GM-CSF deficiency (Online Figure VIA and VIB). Thus, GM-CSF deficiency specifically decreases lesional macrophage and DC apoptosis and plaque necrosis in advance aortic root lesions of WD-fed *Ldlr*$^{-/-}$ mice, which suggested to us a specific mechanism of action.

GM-CSF–Deficient Mice Have Decreased Lesional Cytokines, Including IL-23

To understand the mechanism of decreased apoptosis in the lesions of GM-CSF–deficient mice, we tested several possibilities. If CD11c^{hi} cells were intrinsically more susceptible to apoptosis than CD11c^{lo}F4/80$^+$ cells, then *Csf2*$^{-/-}$*Ldlr*$^{-/-}$ lesions, which have a decrease in CD11c^{hi} cells (above), might simply be populated with a higher percentage of cells that are relatively resistant to apoptosis. However, as shown above, these 2 subpopulations of cells showed similar decreases in apoptosis in the *Csf2*$^{-/-}$*Ldlr*$^{-/-}$ lesions (Online Figure V). In addition, cultured DCs and macrophages exposed to atherosclerosis-relevant proapoptotic factors such as 7-ketocholesterol (7KC) and oxidized low-density lipoprotein showed similar susceptibility to apoptosis (data not shown). A decrease in apoptosis-susceptible neutrophils in the double knockout lesions could also provide an explanation, but the lesions from the 2 groups of mice had similarly low numbers of neutrophils (Online Figure IIIB). Thus, the decrease in lesional apoptosis in *Csf2*$^{-/-}$*Ldlr*$^{-/-}$ lesions cannot be explained by an increase in the ratio of apoptosis-resistant:apoptosis-susceptible cell types.

We next examined whether the lesions of *Csf2*$^{-/-}$*Ldlr*$^{-/-}$ mice had an alteration in cytokines that may lead to a decrease in apoptosis. The mRNA levels of pro- and anti-inflammatory cytokines in the lesions of the 2 groups of mice were quantified by reverse transcriptase quantitative polymerase chain reaction of lesional RNA obtained by laser capture microdissection. We found a significant decrease in the expression of interferon-γ and IL-2 in the GM-CSF–deficient lesions (Figure 3A), consistent with a decrease in lesional T cells (above). Further analysis of T-cell subset mRNA expression indicated a significant decrease in lesional Th1 and Th17 profiles, whereas Th2 and Tregs were unaffected (Figure 3B). The decrease in lesional Th1 cells is consistent with
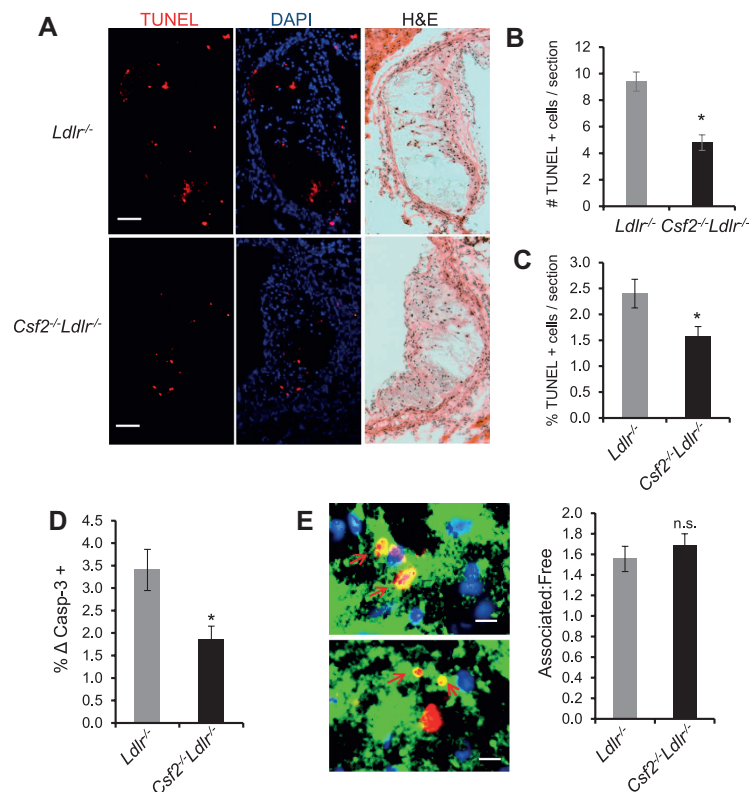
Figure 2. Lesional apoptotic cells are lower in granulocyte macrophage colony-stimulating factor (Csf2)–deficient *Ldlr*⁻/⁻ mice. A, Representative images of terminal deoxynucleotidyl transferase dUTP nick end labeling (TUNEL)–stained aortic root sections of 12-week Western-type diet–fed *Ldlr*⁻/⁻ and *Csf2*⁻/⁻*Ldlr*⁻/⁻ mice (red), with 4′,6-diamidino-2-phenylindole (DAPI)-nuclear counterstain (blue), and their corresponding hematoxylin–eosin (H&E)–stained images. Bar, 25 μm. **B** to **D**, Quantification of lesional TUNEL and activated-caspase-3 data. **E**, In situ efferocytosis was assayed by labeling apoptotic cells with TUNEL (red) and macrophages with anti-F4/80 (green), followed by quantification of the ratio of apoptotic cells that are associated with macrophages vs those that are not (free). The red arrow depicts apoptotic cells that are associated with macrophages. Nuclei were stained with Hoechst dye (blue). Bar, 5 μm. For **B** to **D**, n=10 mice per group; *P<0.05.

the known role of GM-CSF in skewing T-cell differentiation toward a Th1 phenotype. A similar decrease in Th1-cell profile was observed in the spleens of GM-CSF–deficient mice (Online Figure VIIA). However, there were no significant differences between the 2 groups of mice in the numbers of total T cells, CD4⁺ T cells, CD8⁺ T cells, or regulatory T cells in the spleen or peripheral blood (Online Figure VIIB–VIIE). Consistent with a decrease in Th17 cells in the lesions of *Csf2*⁻/⁻*Ldlr*⁻/⁻ mice, expression of the mRNA for IL-17A, the major cytokine produced by Th17 cells, was also decreased in the lesions of this cohort (Figure 3A). Previous studies have shown that IL-23, a cytokine induced by GM-CSF, is critical for Th17-cell differentiation and survival.[3,24] In agreement with these reports, we found decreased levels of IL-23 in the double knockout lesions (Figure 3A and 3C), whereas serum IL-23 levels were unchanged between the 2 groups of mice (Online Figure VIII). Macrophages and DCs are the major producers of IL-23 in atherosclerotic lesions (Online Figure IX), and their production of IL-23 was significantly decreased in the GM-CSF–deficient mice (Online Figure X). Finally, consistent with the lack of changes in the numbers of lesional Tregs and macrophages, lesional *Il10* and *Tgfb* mRNA were similar in *Ldlr*⁻/⁻ mice and *Csf2*⁻/⁻*Ldlr*⁻/⁻ mice (Figure 3A). In summary, the lesions of WD-fed *Csf2*⁻/⁻*Ldlr*⁻/⁻ mice are characterized by decreases in the mRNAs for specific T-cell cytokines, particularly *Il17*, and a decrease in *Il23*.

IL-23 Increases Apoptosis Susceptibility in Cultured Macrophages, and Restoration of IL-23 in *Csf2*⁻/⁻*Ldlr*⁻/⁻ Mice Increases Lesional Apoptosis

IL-17 plays a proapoptotic role in vascular endothelial cells[25] and in cardiomyocytes after ischemia–reperfusion injury,[26] whereas IL-23 has been reported to play a role in apoptosis of

self-reactive thymocytes during T-cell selection[27] and of leukemic cells in B-acute lymphoblastic leukemia.[28] We therefore tested whether IL-17 or IL-23 could induce apoptosis in cultured macrophages under basal conditions or when exposed to 7KC, a proapoptotic oxysterol present in human atherosclerotic lesions.[29,30] Apoptosis was assessed by annexin-V staining, which labels externalized phosphatidylserine on the plasma membrane of apoptotic cells. Treatment of macrophages with IL-17 or IL-23 alone did not lead to a significant increase in the number of annexin-V+ cells (Figure 4A and 4B). Similarly, treatment of macrophages with IL-17 did not result in enhancement of 7KC-induced apoptosis (Figure 4A). However, IL-23 treatment led to a significant, dose-dependent increase in 7KC-induced macrophage apoptosis (Figure 4B; Online Figure XI), and this effect was abrogated by coincubation with a neutralizing antibody against the IL-23 receptor (Figure 4C). The neutralizing effect of the IL-23 receptor antibody was validated by demonstrating blockage of IL-23–induced STAT3 phosphorylation in cultured macrophages (data not shown). IL-12 and IL-23 share a common subunit and certain common functions,[31] but IL-12 did not enhance macrophage apoptosis (Figure 4C). The effect of IL-23 in sensitizing macrophages to apoptosis was not specific to 7-KC: both oxidized low-density lipoprotein[32] and the combination of an endoplasmic reticulum stressor and oxidized phospholipid (thapsigargin and KOdiA-PC)[33] gave similar results (Online Figure XII). In contrast, tumor necrosis factor-α, IL-2, interferon-γ, and IL-6, which are higher in the lesions of *Ldlr*⁻/⁻ versus *Csf2*⁻/⁻*Ldlr*⁻/⁻ mice, did not increase basal or 7KC-induced apoptosis susceptibility in cultured macrophages (Online Figure XIII). Finally, consistent with our in vivo data that GM-CSF-deficient mice have decreased apoptosis of lesional DCs as well as macrophages, we
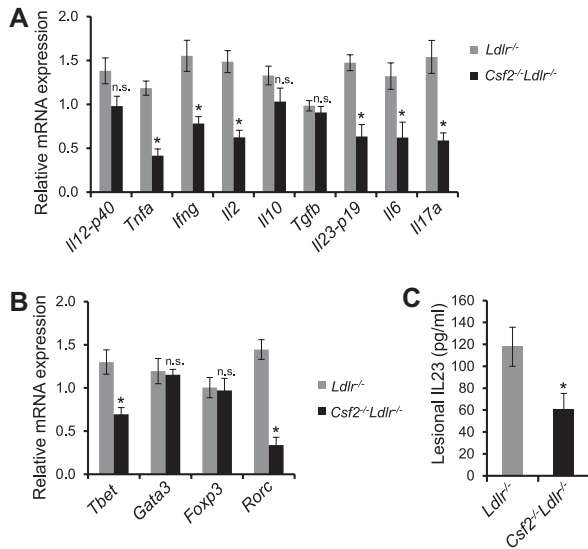
Figure 3. Aortic root lesions of granulocyte macrophage colony-stimulating factor (Csf2)–deficient *Ldlr*$^{-/-}$ mice have lower levels of interleukin (IL)-23. A and **B**, RNA was isolated by laser capture microdissection of lesional cells in 12-week Western-type diet (WD)–fed *Ldlr*$^{-/-}$ and *Csf2*$^{-/-}$*Ldlr*$^{-/-}$ mice, and mRNA of the indicated genes was quantified by reverse transcriptase quantitative polymerase chain reaction. All data are normalized to *Actb* mRNA. n=5 mice per group; *$P<0.05$. **C**, Atherosclerotic lesional extracts obtained from 12-week WD-fed *Ldlr*$^{-/-}$ and *Csf2*$^{-/-}$*Ldlr*$^{-/-}$ mice were assayed for IL-23 by ELISA. n=10 mice per group; *$P<0.05$. TGFβ indicates transforming growth factor-β; and TNFα, tumor necrosis factor-α.

found that cultured bone marrow–dervied DCs demonstrated enhanced susceptibility to 7KC-induced apoptosis in the presence of IL-23 (Online Figure XIV). These combined data demonstrate that IL-23 enhances the susceptibility of macrophages

and DCs to apoptosis induced by certain atherorelevant apoptotic factors in an IL-23 receptor–dependent manner.

To test the role of IL-23 in lesional macrophage apoptosis in vivo, we administered recombinant mouse IL-23 to *Ldlr*$^{-/-}$ or *Csf2*$^{-/-}$*Ldlr*$^{-/-}$ mice as per the scheme illustrated in Figure 5A. The primary aim was to restore lesional IL-23 levels in the GM-CSF–deficient mice and to evaluate the effect of this restoration on lesional cell apoptosis. Using an IL-23 ELISA assay of lesional extracts and a pilot IL-23 dosing experiment, we found a dose of recombinant mouse IL-23 that restored the level of lesional IL-23 in GM-CSF–deficient mice close to the level of lesional IL-23 in control (Veh) *Ldlr*$^{-/-}$ mice (Figure 5B; compare first and fourth bars). Because ELISA is a measure of immunogenic rather than bioactive IL-23, we analyzed the functional activity of IL-23 by measuring the mRNA level of one of its target genes, *Il17a*. Consistent with the ELISA data, *Il17a* mRNA in the lesions of IL-23–treated *Csf2*$^{-/-}$*Ldlr*$^{-/-}$ mice was restored close to the level in control *Ldlr*$^{-/-}$ mice (Figure 5C; compare first and fourth bars). However, restoration of IL-23 levels did not affect the expression levels of other cytokine genes, such as *Tnfa*, *Ifng*, and *Il2*, which remained lower in the GM-CSF–deficient mice (Online Figure XV). Using this dose of IL-23, we found that lesional apoptosis in IL-23–restored *Csf2*$^{-/-}$*Ldlr*$^{-/-}$ mice was increased to the level of that in control *Ldlr*$^{-/-}$ mice (Figure 5D; compare first and fourth bars). Moreover, consistent with the lack of an effect of IL-17 on apoptosis susceptibility in cultured macrophages (above), neutralization of IL-17 activity by administration of anti–IL-17 antibody[34] did not affect lesional cell apoptosis in the IL-23–restored mice or any of the other groups of mice (Figure 5E). As a positive control for the IL-17 antibody, we demonstrated that the level of the IL-17 target mRNA, *Il6*, was decreased in the lesions of anti–IL-17-treated mice (Online Figure XVI). These data, combined with our data with cultured macrophages (above), support the hypothesis that the decrease
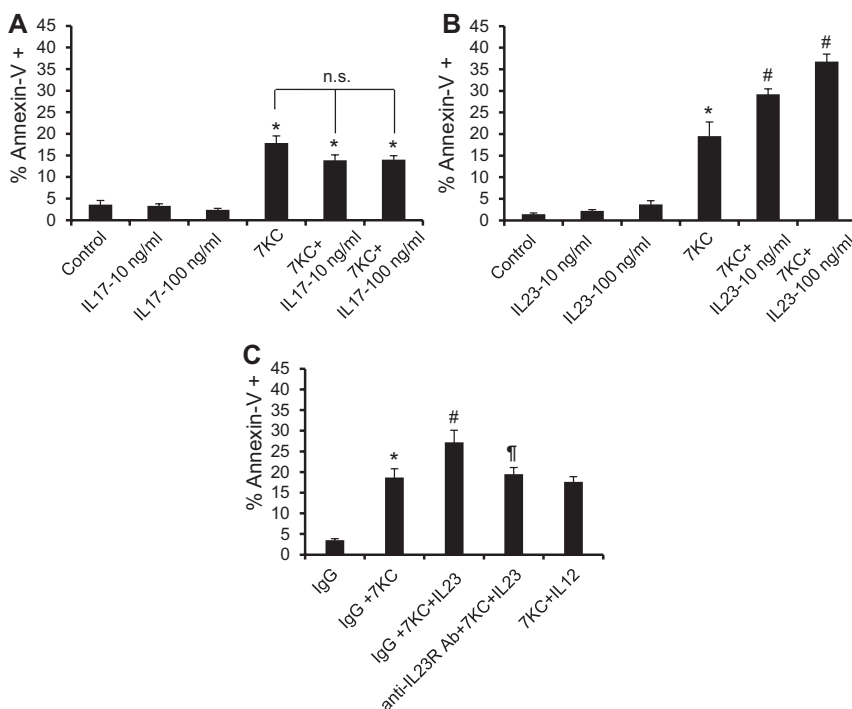
Figure 4. Interleukin (IL)-23 increases the susceptibility of cultured macrophages to 7-ketocholesterol (KC)–induced apoptosis. A, Bone marrow–derived macrophages were treated with the indicated concentration of IL-17, 35 μmol/L 7KC, or a combination of IL-17 and 7KC for 18 hours. Apoptosis was quantified by counting annexin-V–labeled and total cells in fluorescence microscopic images. **B**, Similar to **A**, but the macrophages were treated with IL-23 instead of IL-17. **C**, Similar to B, but some of the groups received either control IgG or neutralizing antibody against the IL-23 receptor (anti-IL-23R, 1 μg/mL) or recombinant IL-12 (100 ng/mL). *$P<0.05$ vs control; #$P<0.05$ vs the 7KC-treated group; ¶$P<0.05$ vs the 7KC+IL-23–treated group. The data are representative of 3 independent experiments.
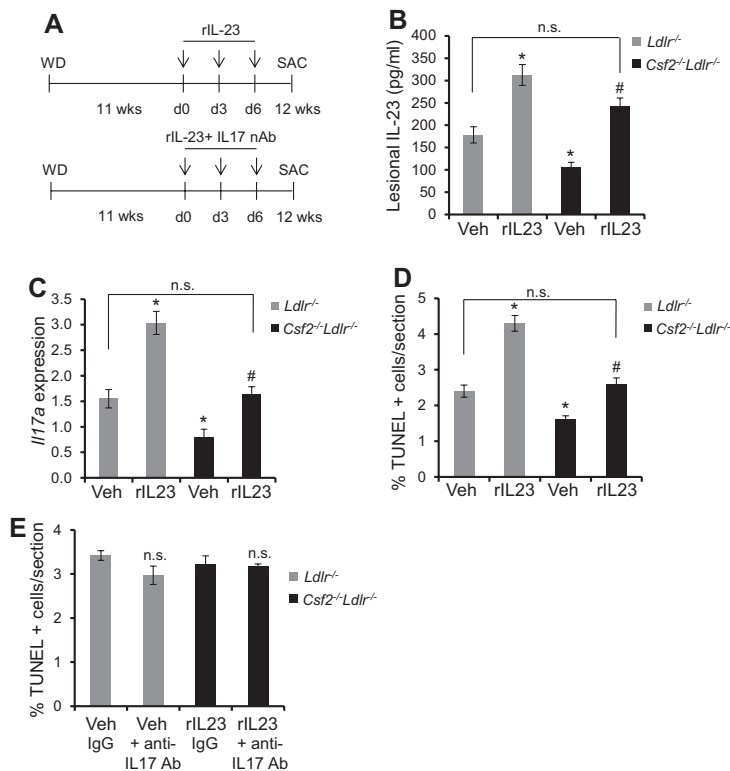
Figure 5. Restoration of interleukin (IL)-23 in *Csf2⁻/⁻Ldlr⁻/⁻* mice increases lesional apoptosis. **A**, Schematic showing the time of intravenous administration of recombinant IL (rIL)-23 (5 μg/kg) or a combination of rIL-23 and anti–IL-17 (100 μg/mouse) neutralizing antibody in Western-type diet (WD)–fed *Ldlr⁻/⁻* and *Csf2⁻/⁻Ldlr⁻/⁻* mice. Control mice were treated with vehicle (Veh). **B**, Extracts of aortic root sections obtained from the indicated groups of mice were assayed for IL-23 by ELISA. **C**, Laser capture microdissection reverse transcriptase quantitative polymerase chain reaction quantification of *Il17a* mRNA, normalized to *Actb*, in the lesions of the indicated groups of mice. **D** and **E**, Percent terminal deoxynucleotidyl transferase dUTP nick end labeling (TUNEL)–positive cells in the atherosclerotic lesions of the indicated groups of mice. For **A** to **D**, n=3 mice for the control group and n=6 mice for the rIL-23–treated group, and for **E**, n=5 mice per group; *$P<0.05$ vs vehicle-treated *Ldlr⁻/⁻* mice; #$P<0.05$ vs vehicle-treated *Csf2⁻/⁻Ldlr⁻/⁻* mice. SAC indicates euthanize.

in lesional IL-23 in *Csf2⁻/⁻Ldlr⁻/⁻* mice plays an important role in the decrease of lesional cell apoptosis in these mice.
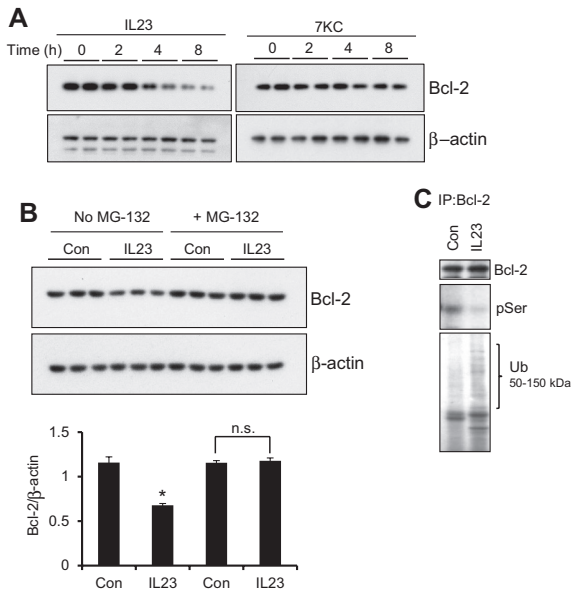
IL-23 Promotes Ubiquitin-Mediated Degradation of the Cell Survival Protein Bcl-2

7KC induces apoptosis in macrophages via activation of the mitochondrial-caspase-9 pathway of apoptosis.[35] We therefore investigated whether this pathway might also be required in IL-23–mediated enhancement of 7KC-induced macrophage apoptosis. Caspase-9 is activated by proteolytic cleavage of the inactive, full-length protein (procaspase-9) into a shorter length active protease.[36] Because activated-caspase-9 protein is short lived in the 7KC-macrophage model, caspase-9 activation is measured by quantifying the disappearance of procaspase 9. We found that IL-23 treatment enhanced 7KC-mediated loss of procaspase-9 (Online Figure XVIIA), indicating enhanced caspase-9 activation. Most importantly, knockdown of caspase-9 blocked apoptosis in 7KC-treated cells and prevented the IL-23 increment in apoptosis (Online Figure XVIIB).

Although the 7KC+IL-23 result does not necessarily prove a direct role for caspase-9 in IL-23 enhancement of apoptosis, because this enhancement requires 7KC-induced apoptosis in the first place, these findings led us to explore further a protein that is known to affect the mitochondrial pathway of apoptosis, Bcl-2.[37] Bcl-2 was of additional interest because of a report showing that it can protect leukemia cells from IL-23–induced apoptosis.[28] In this context, we found that treatment of macrophages and DCs with IL-23, but not 7KC, led to a significant downregulation of Bcl-2 protein expression (Figure 6A; Online Figure XVIIIA). IL-23 did not decease *Bcl2* mRNA (Online Figure XVIIIB), indicating that the observed decrease in Bcl-2 protein

is not because of transcriptional inhibition or decrease in mRNA stability. We next determined whether the decrease in Bcl-2 was regulated by proteasome-mediated degradation, which has been demonstrated in other settings in which Bcl-2 levels are regulated.[38] Consistent with this mechanism, MG-132, a proteasome inhibitor, abrogated the IL-23–mediated decrease in Bcl-2 (Figure 6B). One of the mechanisms by which Bcl-2 is targeted for proteasomal degradation is via dephosphorylation of Ser87, which serves as a signal for polyubiquitination by ubiquitin ligases.[38] Because ubiquitination of endogenous proteins is difficult to detect, we overexpressed full-length mouse Bcl-2 in control and IL-23–treated macrophages and then conducted an immunoprecipitation-immunoblot experiment. The data show a significant decrease in phospho-Ser-Bcl-2 in IL-23–treated macrophages compared with control cells (Figure 6C, middle blot). Moreover, when the same lysates were immunoblotted for ubiquitin, we found that there was an increase in high-molecular weight bands between 50 and 150 kDa in the extracts from IL-23–treated macrophages, indicating that IL-23 promotes polyubiquitination of Bcl-2 (Figure 6C, lower blot). Thus, the ability of IL-23 to promote Bcl-2 dephosphorylation and subsequent ubiquitination is a plausible mechanism for IL-23–mediated Bcl-2 downregulation.

IL-23 Downregulates Bcl-2 and Enhances Apoptosis Susceptibility by Inducing Mitogen-Activated Protein Kinase Phosphatase-1–Mediated Suppression of Extracellular Signal–Related Kinase

Phosphorylation of Bcl-2 is mediated by extracellular signal–related kinase (ERK),[38] and so we tested whether the decrease in phospho-Bcl-2 by IL-23 is caused by a decrease in ERK

A

B

C

Figure 6. Interleukin (IL)-23 induces ubiquitin-mediated degradation of Bcl-2 (B-cell lymphoma 2). A and **B**, Immunoblot of Bcl-2 in macrophages treated with IL-23 (10 ng/mL) or 7-ketocholesterol (7KC; 35 μmol/L) for the indicated times in **A** or for 8 hours in **B** in the absence or presence of the proteasome inhibitor MG-132 (10 μmol/L). β-Actin was used as a loading control. The bar graph represents densitometric analysis of the immunoblot data in **B**. **C**, Macrophages transfected with a plasmid encoding Bcl-2 was treated without (Con) or with IL-23 for 4 hours in the presence of MG-132. Bcl-2 was immunoprecipitated (IP) followed by immunoblotting for Bcl-2, phosphoserine (pSer) and ubiquitin (Ub). *$P<0.05$ vs control; #$P<0.05$ vs 7KC treatment. The data are representative of 3 independent experiments.

activity. Consistent with this scenario, we observed that IL-23 treatment was associated with a decrease in the level of phospho-ERK, the active form of ERK (Figure 7A). In addition, treatment of macrophages with an ERK inhibitor mimicked the effect of IL-23 on decreasing Bcl-2 protein (Online Figure XIXA). The decrease in phospho-ERK could be mediated by decreased phosphorylation by its upstream kinase MEK or by increased dephosphorylation by the phosphatases mitogen-activated protein kinase phosphatase-1 (MKP-1) or MKP-3. Whereas the level of active phospho-MEK in IL-23–treated macrophages was similar to that in control cells (Online Figure XIXB), MKP-1 protein was increased in IL-23–treated macrophages (Figure 7B). MKP-3 levels were similar between the 2 groups of macrophages (data not shown).

We next tested whether the increase in MKP-1 expression was causally related to ERK dephosphorylation, Bcl-2 degradation, and increased apoptosis susceptibility in IL-23–treated macrophages using MKP-1 small interfering RNA. As predicted by the hypothesis that MKP-1 is a key upstream mediator in the IL-23 pathway, silencing MKP-1 abrogated the decrease in phospho-ERK and Bcl-2 expression (Figure 7C). Most importantly, knockdown of MKP-1 protected macrophages from the increment in apoptosis observed in IL-23/7KC–treated macrophages compared with 7KC-treated macrophages (Figure 7D).

To test the relevance of the MKP-1 model to advanced atherosclerosis, we quantified lesional MKP-1 expression by

immunohistochemistry. The data show a significantly lower level of MKP-1 in the lesions of GM-CSF–deficient $Ldlr^{-/-}$ mice (Figure 7E; Online Figure XXA). As a control for the specificity of the antibody, we observed significantly lower expression of MKP-1 in macrophages transfected with small interfering RNA against MKP-1 (Online Figure XXB). In addition, Western blotting for MKP-1 in extracts obtained from sections of aortic root demonstrated significantly lower expression of MKP-1 in the GM-CSF–deficient lesions (Online Figure XXC). Consistent with the decrease in MKP-1, the lesions of $Csf2^{-/-}Ldlr^{-/-}$ mice demonstrated increased levels of Bcl-2 expression as measured by immunohistochemistry (Figure 7F; Online Figure XXI). Finally, both the decrease in lesional MKP-1 and the increase in lesional Bcl-2 in GM-CSF–deficient mice could be reversed by exogenous administration of recombinant mouse IL-23 (Figure 7G and 7F; Online Figure XXII). In summary, IL-23 increases apoptosis susceptibility in 7KC-treated macrophages through upregulation of MKP-1. MKP-1 decreases ERK-mediated phosphorylation of Bcl-2, leading to polyubiquitination and proteasomal degradation of Bcl-2 and a subsequent increase in apoptosis susceptibility.

IL-23-MKP-1 Pathway Enhances Reactive Oxygen Species in 7KC-Treated Macrophages and in Advanced Atherosclerotic Lesions

Oxidative stress and the generation of various reactive oxygen species (ROS) and ROS-modified proteins and lipids are key features of advanced plaque progression.[39,40] In cultured primary macrophages exposed to atherorelevant factors, including 7KC, ROS mediated by NADPH oxidase promotes apoptosis.[29,30] Interestingly, one of the mechanisms by which Bcl-2 can exert its antiapoptotic activity is via its role as an antioxidant.[41,42] In the context of these previous findings, we hypothesized that the IL-23–induced decrease in Bcl-2 might result in enhanced ROS generation, which in turn would further drive apoptosis susceptibility in macrophages exposed to atherorelevant proapoptotic factors. To address this hypothesis, we incubated macrophages with 7KC in the absence or presence of IL-23 and then probed the cells with CellROX Deep Red, which fluoresces in the cytoplasm when exposed to ROS.[43] Similar to the apoptosis findings, IL-23 alone did not induce ROS in macrophages, but it enhanced ROS in the presence of 7KC (Figure 8A; Online Figure XXIIIA). In contrast, IL-23 did not affect 7KC-induced ROS in the mitochondria (data not shown), which was assayed using the mitochondrial ROS probe mitoSOX.[40]

Next, to assess whether the increase in ROS on IL-23 treatment was a consequence of the decrease in Bcl-2,[41,42] we blocked Bcl-2 degradation using *Mkp1* small interfering RNA (above). We found that the increment in ROS that occurs when IL-23 is added to 7KC-treated macrophages was abrogated by silencing MKP-1 (Figure 8B; Online Figure XXIIIB). Conversely, silencing Bcl2 mimicked IL-23 in terms of its ability to increase the ROS response in 7KC-treated macrophages (Figure 8C; Online Figure XXIIIC and XXIIID). The question as to whether the IL-23–mediated increment in ROS is causally important in its ability to enhance apoptosis susceptibility in 7KC-treated macrophages is difficult to address, because blocking ROS in these cells,
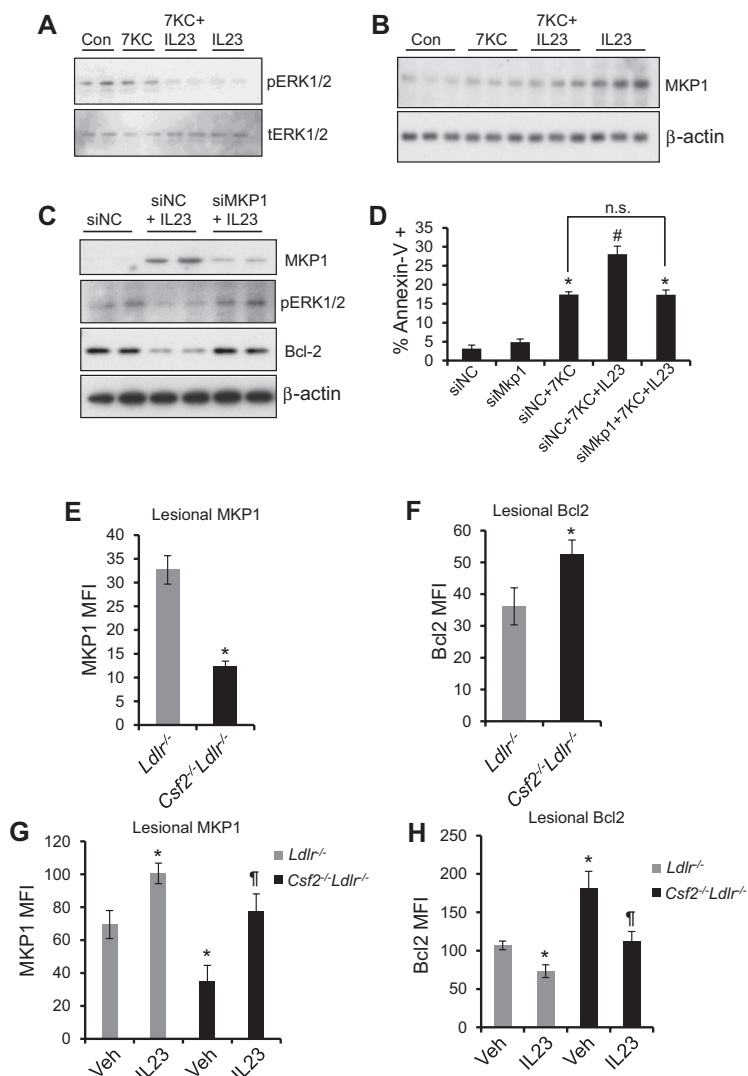
Figure 7. Evidence that an increase in mitogen-activated protein kinase phosphatase-1 (MKP-1) links granulocyte macrophage colony-stimulating factor (Csf2)/interleukin (IL)-23 to decreased Bcl-2 (B-cell lymphoma 2) and apoptosis in macrophages and in atherosclerotic lesions. **A**, Macrophages treated with 7-ketocholesterol (7KC) alone, IL-23 alone, or the combination of 7KC and IL-23 for 30 minutes were probed for phospho-extracellular signal–related kinase (pERK) or total ERK (tERK)1/2 by immunoblotting. **B**, Immunoblot of MKP-1 in macrophages treated with 7KC alone, IL-23 alone, or the combination of 7KC and IL-23 for 4 hours. **C**, Macrophages were transfected with negative control small interfering RNA (siNC) or siRNA against MKP-1 (siMkp1) and then treated 48 hours later without or with IL-23 for 8 hours. Whole cell lysates were immunoblotted for MKP-1, pERK1/2, Bcl-2, and β-actin. **D**, Macrophages transfected with siNC or siMkp1 were treated with 7KC or a combination of 7KC and IL-23 for 18 hours followed by quantification of apoptosis by microscopic analysis of annexin-V–labeled macrophages. **E** to **H**, Immunofluorescence quantification (mean fluorescence intensity, MFI) of MKP-1 and Bcl-2 in F4/80+ macrophage-rich regions of aortic root atherosclerotic lesions. n=6 mice per group. **G** and **H**, The indicated groups of mice were treated with saline (Veh) or recombinant IL (rIL)-23 (5 μg/kg). **D**, The data are representative of 3 independent experiments. In **E** and **F**, n=6 mice per group, and in **G** and **H**, n=3 mice for the control group and n=6 mice for rIL-23–treated group; *$P<0.05$ vs control or $Ldlr^{-/-}$ mice; #$P<0.05$ vs 7KC treatment; ¶$P<0.05$ vs vehicle-treated $Csf2^{-/-}Ldlr^{-/-}$ mice.

for example, using NADPH oxidase 2–deficient macrophages, blocks 7KC-induced apoptosis,[30] which by itself would negate the IL-23 effect. Nonetheless, we did find that IL-23 was unable to enhance apoptosis above the suppressed level seen in 7KC-treated NADPH oxidase 2–deficient macrophages (data not shown). Finally, to determine the relevance of these findings in atherosclerosis, we analyzed lesional ROS by staining aortic root sections obtained from WD-fed $Ldlr^{-/-}$ and $Csf2^{-/-}Ldlr^{-/-}$ mice with the fluorescent superoxide sensor dihydroethidium. Consistent with the cultured macrophage data, we observed decreased dihydroethidium staining in the lesions of GM-CSF–deficient mice (Figure 8D; Online Figure XXIVA). Moreover, similar to the lesional apoptosis data in Figure 5D, this decrease in lesional ROS in the $Csf2^{-/-}Ldlr^{-/-}$ mice was reversed by treating the mice with a restorative level of recombinant mouse IL-23 (Figure 8E; Online Figure XXIVB). These combined findings support a model in which the GM-CSF-IL-23-MKP-1 pathway promotes the degradation of Bcl-2, which increases apoptosis susceptibility by activating the mitochondrial-caspase 9 pathway of apoptosis as well as by enhancing ROS accumulation (Figure 8F).

Discussion

Earlier studies examining the function of GM-CSF in atherosclerosis have focused on its roles in myeloid cell differentiation and proliferation. For example, GM-CSF was demonstrated to be essential for the proliferation of CD11c^{hi} cells in nascent atherosclerotic lesions,[44] which is consistent with the ability of GM-CSF to stimulate the differentiation of cultured DCs. However, a recent study demonstrated that GM-CSF is not necessary for differentiation of inflammatory DCs derived from monocytes.[45] Thus, it is possible that GM-CSF affects a specific subset of resident conventional DCs in the subendothelial space of healthy arteries or the intima of early atherosclerotic lesions. Consistent with this idea, we observed only a modest decrease in CD11c^{hi}MHC-II^{hi} DCs in established atherosclerotic lesions of GM-CSF–deficient mice.

In terms of atherosclerosis per se, the role of GM-CSF seems to be influenced by the model used and the focus of the study. In particular, studies using mice that completely lack apolipoprotein E in all cells or in bone marrow–derived cells, which is known to affect immune cell function[46,47] and hematopoietic stem cell proliferation[48] have shown complex
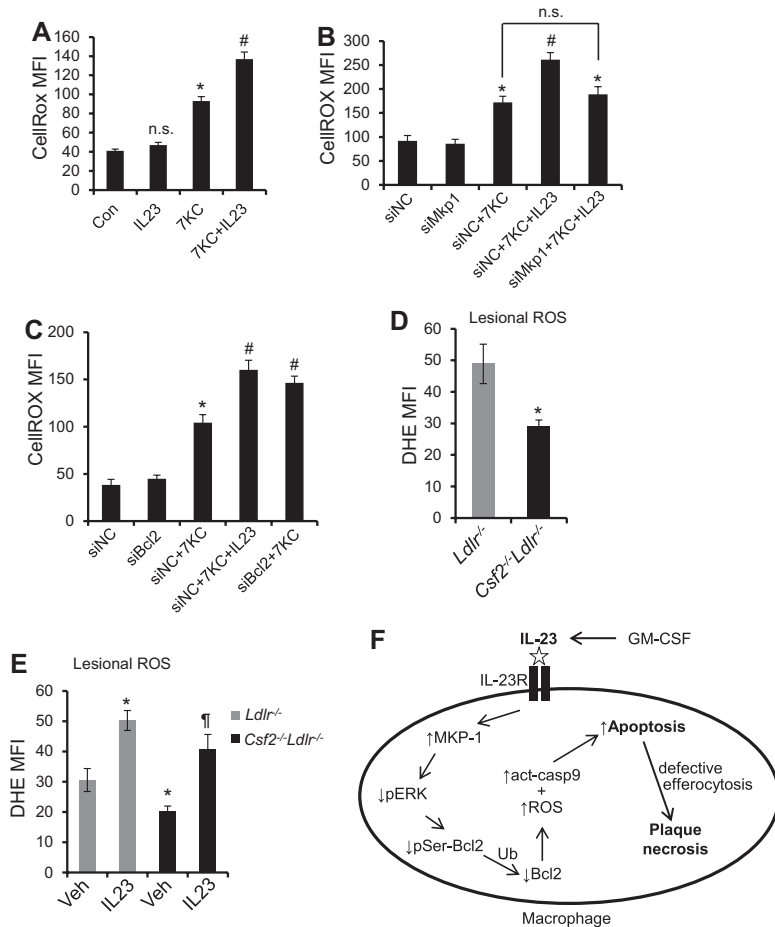
Figure 8. Lesional reactive oxygen species (ROS) is lower in granulocyte macrophage colony-stimulating factor (GM-CSF)–deficient *Ldlr*^{−/−} mice and is reversed on restoration of interleukin (IL)-23. A to C, Flow-cytometric measurement of ROS using an ROS-sensitive probe, CellROX, in macrophages subjected to the indicated treatments for 6 hours. **D,** Quantification of lesional ROS by microscopic analysis of dihydroethidium (DHE) staining in 12-week Western-type diet (WD)–fed *Ldlr*^{−/−} and *Csf2*^{−/−}*Ldlr*^{−/−} mice and (**E**) in *Ldlr*^{−/−} and *Csf2*^{−/−}*Ldlr*^{−/−} mice treated with saline (Veh) or recombinant IL (rIL)-23 (5 μg/kg). n=3 mice for control group and n=6 mice for rIL-23–treated group; *P<0.05 vs control or *Ldlr*^{−/−} mice; #P<0.05 vs the 7-ketocholesterol (7KC)–treated group; ¶P<0.05 vs *Csf2*^{−/−}*Ldlr*^{−/−} mice. **F,** Schematic summary of the mechanism by which the GM-CSF-IL-23 pathway enhances apoptosis susceptibility in macrophages. See text for details. MFI indicates mean fluorescence intensity; pERK, phospho-extracellular signal–related kinase; pSer, phosphoserine; and Ub, ubiquitination.

effects that may be specific to models lacking apolipoprotein E. As an example of the complexity, exogenous administration of GM-CSF to *Apoe*^{−/−} mice was reported to increase atherosclerotic lesion size,[14] whereas deficiency of GM-CSF in an *Apoe*^{−/−} background was also associated with larger lesion size and increased macrophage content, which was attributed to a decrease in macrophage perixosome proliferator-activated receptor (PPAR)-γ and ABCA1.[7] In contrast, in WD-fed *Ldlr*^{−/−} model used here, which has lipoprotein profiles similar to dyslipidemic humans and do not have adverse immune effects, GM-CSF deficiency did not affect macrophage *Pparg*, *Abca1*, or *Abcg1* expression in lesional macrophages (unpublished data). Moreover, in WD-fed *Ldlr*^{−/−} mice, we found that GM-CSF deficiency had no significant effect on aortic root lesion size per se, which agrees in principle with another group showing only a modest effect in females but not in males.[13] Rather, as demonstrated here, the dominant effect of GM-CSF in *Ldlr*^{−/−} mice is enhancement of macrophage apoptosis in advanced atherosclerosis by a specific mechanism related to its ability to induce IL-23 production.

The results of the current study underscore the importance of the cytokine-inducing role of GM-CSF in atherosclerosis, which in this case involves a particular cytokine, IL-23, that promotes macrophage apoptosis. Under physiological conditions, GM-CSF–induced production of IL-23 and subsequent macrophage apoptosis may act as a feedback mechanism to control immune cell populations or to prevent excessive

inflammation. In that setting, the apoptotic macrophages would be rapidly cleared by neighboring phagocytes (efferocytosis), which prevents both secondary necrosis and generation of proinflammatory damage-associated molecular patterns and also activates anti-inflammatory signaling pathways in the efferocytes themselves.[49] However, in advanced atherosclerotic lesions, efferocytosis is defective,[50] and so processes that increase apoptosis promote necrosis and inflammation, which, as demonstrated here, is the case with GM-CSF–induced IL-23.

The link between GM-CSF and IL-23 has been explored most extensively in the setting of autoimmune disorders, where a GM-CSF/IL-23/Th17 axis has been demonstrated to play a major role in disease exacerbation.[3,24] Accordingly, anti–GM-CSF, anti–IL-23, and anti–IL-17 therapies are currently under investigation for treatment of these diseases.[12,51] In these disorders, mechanistic studies have focused on the role of IL-23 in promoting Th17-cell survival and Th17-mediated IL-17 production. In advanced atherosclerosis, however, the pathogenic effect of IL-23 seems to be largely independent of IL-17 generation, as neutralization of IL-17 activity did not block IL-23–induced macrophage apoptosis or plaque necrosis. Moreover, IL-23, but not IL-17, increased apoptosis in 7KC-treated macrophages. IL-23 has been shown previously to induce apoptosis in self-reactive thymocytes,[27] and, at high concentration, in B-acute lymphoblastic leukemia cells.[28] In B-acute lymphoblastic leukemia cells, like macrophages, the proapoptotic mechanism of IL-23 involves downregulation of

Bcl-2. In B-acute lymphoblastic leukemia cells, however, Bcl-2 downregulation is mediated by a microRNA, miR15a,[28] whereas in macrophages, Bcl-2 downregulation is mediated by the proteasome after MKP-1–mediated Bcl-2 dephosphorylation.

Our laboratory has previously shown that atherosclerosis-prone mice lacking macrophage Bcl-2 have increased lesional macrophage apoptosis and increased necrotic area,[52] which demonstrates that Bcl-2 is critical for macrophage survival in advanced atherosclerosis. The current study provides a pathophysiolgically relevant context for this effect, namely, GM-CSF/IL-23–mediated downregulation of macrophage Bcl-2. The classic role of Bcl-2 is suppression of the mitochondrial-caspase-9 pathway of apoptosis,[37] but our data as well as previous studies[41,42] suggest that Bcl-2 can also suppress intracellular oxidant stress. Given the role of ROS in macrophage apoptosis,[18] we propose the GM-CSF/IL-23 pathway, through destabilizing Bcl-2, promotes apoptosis susceptibility in macrophages by increasing both caspase-9 activity and intracellular ROS. The precise mechanism through which Bcl-2 regulates intracellular ROS in other models is not well understood, but there is evidence that it may involve upregulation of superoxide dismutase and catalase,[42] as well as direct binding to the antioxidant GSH.[53] How Bcl-2 regulates cytosolic ROS in macrophages in the setting of advanced atherosclerosis will require further study, but we speculate it may involve suppression of NADPH oxidase.[30,54]

Stimuli other than GM-CSF might also increase the generation of IL-23 by macrophages and DCs in atherosclerotic lesions. For example, IL-23 production by DCs is induced by the endoplasmic reticulum stress effector C-EBP homologous protein (CHOP), which binds to a specific promoter region on IL-23 gene.[55] We have demonstrated previously that endoplasmic reticulum stress–induced CHOP plays an important role in macrophage apoptosis and plaque necrosis in advanced atherosclerotic lesions.[56] Whether the proapoptotic effects of endoplasmic reticulum stress on lesional macrophages is mediated, in part, via induction of IL-23 remains to be explored. In addition, Ataxia telangiectasia mutated kinase represses production of IL-23 by DCs,[57] and atherosclerosis is exacerbated in mice lacking Ataxia telangiectasia mutated[58] and in humans with single nucleotide polymorphisms[59] or mutations in Ataxia telangiectasia mutated.[60] The potential link between these observations and excessive IL-23 production thus represents another area of future investigation based on the new findings and pathway described herein.

The results of several preclinical studies and a small human study raise the possibility that exogenously administered recombinant GM-CSF might be proatherogenic and promote coronary artery disease (CAD).[9,10,14] The current data raise the possibility that GM-CSF–induced IL-23 could be involved in these findings. Indeed, a small human study comparing serum IL-23 and IL-17 levels in patients with CAD versus healthy subjects demonstrated that serum IL-23 levels were associated strongly with CAD.[61] This association requires replication and could simply reflect a noncausative, marker-related phenomenon, but the data herein raise the possibility that IL-23 itself could be causative. With these studies in mind, and given the mechanistic insight of the current study, it would be interesting to determine whether patients receiving anti–IL-23 therapy for the treatment of rheumatoid arthritis accrue additional cardiovascular benefits because of decreased plaque necrosis. If so, one could imagine a future therapeutic strategy in which IL-23 or its downstream proapoptotic mediators are neutralized in high-risk patients with the goal of preventing plaque necrosis and subsequent acute cardiovascular clinical events.

Disclosures

None.

References

1. Stanley E, Lieschke GJ, Grail D, Metcalf D, Hodgson G, Gall JA, Maher DW, Cebon J, Sinickas V, Dunn AR. Granulocyte/macrophage colony-stimulating factor-deficient mice show no major perturbation of hematopoiesis but develop a characteristic pulmonary pathology. *Proc Natl Acad Sci USA*. 1994;91:5592–5596.
2. Brissette WH, Baker DA, Stam EJ, Umland JP, Griffiths RJ. GM-CSF rapidly primes mice for enhanced cytokine production in response to LPS and TNF. *Cytokine*. 1995;7:291–295.
3. Sonderegger I, Iezzi G, Maier R, Schmitz N, Kurrer M, Kopf M. GM-CSF mediates autoimmunity by enhancing IL-6-dependent Th17 cell development and survival. *J Exp Med*. 2008;205:2281–2294.
4. Fleetwood AJ, Lawrence T, Hamilton JA, Cook AD. Granulocyte-macrophage colony-stimulating factor (CSF) and macrophage CSF-dependent macrophage phenotypes display differences in cytokine profiles and transcription factor activities: implications for CSF blockade in inflammation. *J Immunol*. 2007;178:5245–5252.
5. Moore KJ, Tabas I. Macrophages in the pathogenesis of atherosclerosis. *Cell*. 2011;145:341–355.
6. Biwa T, Hakamata H, Sakai M, Miyazaki A, Suzuki H, Kodama T, Shichiri M, Horiuchi S. Induction of murine macrophage growth by oxidized low density lipoprotein is mediated by granulocyte macrophage colony-stimulating factor. *J Biol Chem*. 1998;273:28305–28313.
7. Ditiatkovski M, Toh BH, Bobik A. GM-CSF deficiency reduces macrophage PPAR-gamma expression and aggravates atherosclerosis in ApoE-deficient mice. *Arterioscler Thromb Vasc Biol*. 2006;26:2337–2344.
8. Plenz G, Koenig C, Severs NJ, Robenek H. Smooth muscle cells express granulocyte-macrophage colony-stimulating factor in the undiseased and atherosclerotic human coronary artery. *Arterioscler Thromb Vasc Biol*. 1997;17:2489–2499.
9. Zbinden S, Zbinden R, Meier P, Windecker S, Seiler C. Safety and efficacy of subcutaneous-only granulocyte-macrophage colony-stimulating factor for collateral growth promotion in patients with coronary artery disease. *J Am Coll Cardiol*. 2005;46:1636–1642.
10. Shindo J, Ishibashi T, Yokoyama K, Nakazato K, Ohwada T, Shiomi M, Maruyama Y. Granulocyte-macrophage colony-stimulating factor prevents the progression of atherosclerosis via changes in the cellular and extracellular composition of atherosclerotic lesions in watanabe heritable hyperlipidemic rabbits. *Circulation*. 1999;99:2150–2156.
11. Metcalf D. The colony-stimulating factors and cancer. *Nat Rev Cancer*. 2010;10:425–434.
12. Cornish AL, Campbell IK, McKenzie BS, Chatfield S, Wicks IP. G-CSF and GM-CSF as therapeutic targets in rheumatoid arthritis. *Nat Rev Rheumatol*. 2009;5:554–559.

13. Shaposhnik Z, Wang X, Weinstein M, Bennett BJ, Lusis AJ. Granulocyte macrophage colony-stimulating factor regulates dendritic cell content of atherosclerotic lesions. *Arterioscler Thromb Vasc Biol*. 2007;27:621–627.

14. Haghighat A, Weiss D, Whalin MK, Cowan DP, Taylor WR. Granulocyte colony-stimulating factor and granulocyte macrophage colony-stimulating factor exacerbate atherosclerosis in apolipoprotein E-deficient mice. *Circulation*. 2007;115:2049–2054.

15. Virmani R, Burke AP, Farb A, Kolodgie FD. Pathology of the vulnerable plaque. *J Am Coll Cardiol*. 2006;47:C13–C18.

16. Tabas I. Macrophage death and defective inflammation resolution in atherosclerosis. *Nat Rev Immunol*. 2010;10:36–46.

17. Barry-Lane PA, Patterson C, van der Merwe M, Hu Z, Holland SM, Yeh ET, Runge MS. p47phox is required for atherosclerotic lesion progression in ApoE(-/-) mice. *J Clin Invest*. 2001;108:1513–1522.

18. Bennett MR. Reactive oxygen species and death: oxidative DNA damage in atherosclerosis. *Circ Res*. 2001;88:648–650.

19. Subramanian M, Thorp E, Hansson GK, Tabas I. Treg-mediated suppression of atherosclerosis requires MYD88 signaling in DCs. *J Clin Invest*. 2013;123:179–188.

20. Liao X, Sluimer JC, Wang Y, Subramanian M, Brown K, Pattison JS, Robbins J, Martinez J, Tabas I. Macrophage autophagy plays a protective role in advanced atherosclerosis. *Cell Metab*. 2012;15:545–553.

21. Schrijvers DM, De Meyer GR, Kockx MM, Herman AG, Martinet W. Phagocytosis of apoptotic cells by macrophages is impaired in atherosclerosis. *Arterioscler Thromb Vasc Biol*. 2005;25:1256–1261.

22. Thorp E, Cui D, Schrijvers DM, Kuriakose G, Tabas I. Mertk receptor mutation reduces efferocytosis efficiency and promotes apoptotic cell accumulation and plaque necrosis in atherosclerotic lesions of apoe-/- mice. *Arterioscler Thromb Vasc Biol*. 2008;28:1421–1428.

23. Subramanian M, Tabas I. Dendritic cells in atherosclerosis. *Semin Immunopathol*. 2014;36:93–102.

24. McGeachy MJ. GM-CSF: the secret weapon in the T(H)17 arsenal. *Nat Immunol*. 2011;12:521–522.

25. Zhu F, Wang Q, Guo C, Wang X, Cao X, Shi Y, Gao F, Ma C, Zhang L. IL-17 induces apoptosis of vascular endothelial cells: a potential mechanism for human acute coronary syndrome. *Clin Immunol*. 2011;141:152–160.

26. Liao YH, Xia N, Zhou SF, Tang TT, Yan XX, Lv BJ, Nie SF, Wang J, Iwakura Y, Xiao H, Yuan J, Jevallee H, Wei F, Shi GP, Cheng X. Interleukin-17A contributes to myocardial ischemia/reperfusion injury by regulating cardiomyocyte apoptosis and neutrophil infiltration. *J Am Coll Cardiol*. 2012;59:420–429.

27. Li H, Wu Q, Yang P, Cua D, Hsu H-C, Mountz J. Il-23 induces apoptosis of self-reactive thymocytes in thymic negative selection by an rorc dependent mechanism. *J Immunol*. 2011;186:64.19.

28. Cocco C, Canale S, Frasson C, Di Carlo E, Ognio E, Ribatti D, Prigione I, Basso G, Airoldi I. Interleukin-23 acts as antitumor agent on childhood B-acute lymphoblastic leukemia cells. *Blood*. 2010;116:3887–3898.

29. Myoishi M, Hao H, Minamino T, Watanabe K, Nishihira K, Hatakeyama K, Asada Y, Okada K, Ishibashi-Ueda H, Gabbiani G, Bochaton-Piallat ML, Mochizuki N, Kitakaze M. Increased endoplasmic reticulum stress in atherosclerotic plaques associated with acute coronary syndrome. *Circulation*. 2007;116:1226–1233.

30. Li G, Scull C, Ozcan L, Tabas I. NADPH oxidase links endoplasmic reticulum stress, oxidative stress, and PKR activation to induce apoptosis. *J Cell Biol*. 2010;191:1113–1125.

31. Belladonna ML, Renauld JC, Bianchi R, Vacca C, Fallarino F, Orabona C, Fioretti MC, Grohmann U, Puccetti P. IL-23 and IL-12 have overlapping, but distinct, effects on murine dendritic cells. *J Immunol*. 2002;168:5448–5454.

32. Terasaka N, Wang N, Yvan-Charvet L, Tall AR. High-density lipoprotein protects macrophages from oxidized low-density lipoprotein-induced apoptosis by promoting efflux of 7-ketocholesterol via ABCG1. *Proc Natl Acad Sci USA*. 2007;104:15093–15098.

33. Seimon TA, Nadolski MJ, Liao X, Magallon J, Nguyen M, Feric NT, Koschinsky ML, Harkewicz R, Witztum JL, Tsimikas S, Golenbock D, Moore KJ, Tabas I. Atherogenic lipids and lipoproteins trigger CD36-TLR2-dependent apoptosis in macrophages undergoing endoplasmic reticulum stress. *Cell Metab*. 2010;12:467–482.

34. Cheng X, Taleb S, Wang J, et al. Inhibition of IL-17A in atherosclerosis. *Atherosclerosis*. 2011;215:471–474.

35. Biasi F, Leonarduzzi G, Vizio B, Zanetti D, Sevanian A, Sottero B, Verde V, Zingaro B, Chiarpotto E, Poli G. Oxysterol mixtures

36. Pop C, Timmer J, Sperandio S, Salvesen GS. The apoptosome activates caspase-9 by dimerization. *Mol Cell*. 2006;22:269–275.

37. Gross A, McDonnell JM, Korsmeyer SJ. BCL-2 family members and the mitochondria in apoptosis. *Genes Dev*. 1999;13:1899–1911.

38. Breitschopf K, Haendeler J, Malchow P, Zeiher AM, Dimmeler S. Posttranslational modification of Bcl-2 facilitates its proteasome-dependent degradation: molecular characterization of the involved signaling pathway. *Mol Cell Biol*. 2000;20:1886–1896.

39. Martinet W, Knaapen MW, De Meyer GR, Herman AG, Kockx MM. Oxidative DNA damage and repair in experimental atherosclerosis are reversed by dietary lipid lowering. *Circ Res*. 2001;88:733–739.

40. Wang Y, Wang GZ, Rabinovitch PS, Tabas I. Macrophage mitochondrial oxidative stress promotes atherosclerosis and nuclear factor-κB-mediated inflammation in macrophages. *Circ Res*. 2014;114:421–433.

41. Hockenbery DM, Oltvai ZN, Yin XM, Milliman CL, Korsmeyer SJ. Bcl-2 functions in an antioxidant pathway to prevent apoptosis. *Cell*. 1993;75:241–251.

42. Deng X, Gao F, May WS Jr. Bcl2 retards G1/S cell cycle transition by regulating intracellular ROS. *Blood*. 2003;102:3179–3185.

43. Grailer JJ, Canning BA, Kalbitz M, Haggadone MD, Dhond RM, Andjelkovic AV, Zetoune FS, Ward PA. Critical role for the NLRP3 inflammasome during acute lung injury. *J Immunol*. 2014;192:5974–5983.

44. Zhu SN, Chen M, Jongstra-Bilen J, Cybulsky MI. GM-CSF regulates intimal cell proliferation in nascent atherosclerotic lesions. *J Exp Med*. 2009;206:2141–2149.

45. Greter M, Helft J, Chow A, et al. GM-CSF controls nonlymphoid tissue dendritic cell homeostasis but is dispensable for the differentiation of inflammatory dendritic cells. *Immunity*. 2012;36:1031–1046.

46. Curtiss LK, Boisvert WA. Apolipoprotein E and atherosclerosis. *Curr Opin Lipidol*. 2000;11:243–251.

47. Wang M, Subramanian M, Abramowicz S, Murphy AJ, Gonen A, Witztum J, Welch C, Tabas I, Westerterp M, Tall AR. Interleukin-3/granulocyte macrophage colony-stimulating factor receptor promotes stem cell expansion, monocytosis, and atheroma macrophage burden in mice with hematopoietic ApoE deficiency. *Arterioscler Thromb Vasc Biol*. 2014;34:976–984.

48. Murphy AJ, Akhtari M, Tolani S, Pagler T, Bijl N, Kuo CL, Wang M, Sanson M, Abramowicz S, Welch C, Bochem AE, Kuivenhoven JA, Yvan-Charvet L, Tall AR. ApoE regulates hematopoietic stem cell proliferation, monocytosis, and monocyte accumulation in atherosclerotic lesions in mice. *J Clin Invest*. 2011;121:4138–4149.

49. Fadok VA, Bratton DL, Konowal A, Freed PW, Westcott JY, Henson PM. Macrophages that have ingested apoptotic cells in vitro inhibit proinflammatory cytokine production through autocrine/paracrine mechanisms involving TGF-beta, PGE2, and PAF. *J Clin Invest*. 1998;101:890–898.

50. Tabas I. Consequences and therapeutic implications of macrophage apoptosis in atherosclerosis: the importance of lesion stage and phagocytic efficiency. *Arterioscler Thromb Vasc Biol*. 2005;25:2255–2264.

51. Tausend W, Downing C, Tyring S. Systematic review of interleukin-12, interleukin-17, and interleukin-23 pathway inhibitors for the treatment of moderate-to-severe chronic plaque psoriasis: ustekinumab, briakinumab, tildrakizumab, guselkumab, secukinumab, ixekizumab, and brodalumab. *J Cutan Med Surg*. 2014;18:1–14.

52. Thorp E, Li Y, Bao L, Yao PM, Kuriakose G, Rong J, Fisher EA, Tabas I. Brief report: increased apoptosis in advanced atherosclerotic lesions of Apoe-/- mice lacking macrophage Bcl-2. *Arterioscler Thromb Vasc Biol*. 2009;29:169–172.

53. Zimmermann AK, Loucks FA, Schroeder EK, Bouchard RJ, Tyler KL, Linseman DA. Glutathione binding to the Bcl-2 homology-3 domain groove: a molecular basis for Bcl-2 antioxidant function at mitochondria. *J Biol Chem*. 2007;282:29296–29304.

54. Judkins CP, Diep H, Broughton BR, Mast AE, Hooker EU, Miller AA, Selemidis S, Dusting GJ, Sobey CG, Drummond GR. Direct evidence of a role for Nox2 in superoxide production, reduced nitric oxide bioavailability, and early atherosclerotic plaque formation in ApoE-/- mice. *Am J Physiol Heart Circ Physiol*. 2010;298:H24–H32.

55. Goodall JC, Wu C, Zhang Y, McNeill L, Ellis L, Saudek V, Gaston JS. Endoplasmic reticulum stress-induced transcription factor, CHOP, is crucial for dendritic cell IL-23 expression. *Proc Natl Acad Sci USA*. 2010;107:17698–17703.

prevent proapoptotic effects of 7-ketocholesterol in macrophages: implications for proatherogenic gene modulation. *FASEB J*. 2004;18:693–695.

56. Thorp E, Li G, Seimon TA, Kuriakose G, Ron D, Tabas I. Reduced apoptosis and plaque necrosis in advanced atherosclerotic lesions of Apoe-/- and Ldlr-/- mice lacking CHOP. *Cell Metab*. 2009;9:474–481.

57. Wang Q, Franks HA, Lax SJ, El Refaee M, Malecka A, Shah S, Spendlove I, Gough MJ, Seedhouse C, Madhusudan S, Patel PM, Jackson AM. The ataxia telangiectasia mutated kinase pathway regulates IL-23 expression by human dendritic cells. *J Immunol*. 2013;190: 3246–3255.

58. Schneider JG, Finck BN, Ren J, Standley KN, Takagi M, Maclean KH, Bernal-Mizrachi C, Muslin AJ, Kastan MB, Semenkovich CF.

ATM-dependent suppression of stress signaling reduces vascular disease in metabolic syndrome. *Cell Metab*. 2006;4:377–389.

59. Li S, Zhang L, Chen T, Tian B, Deng X, Zhao Z, Yuan P, Dong B, Zhang Y, Mo X. Functional polymorphism rs189037 in the promoter region of ATM gene is associated with angiographically characterized coronary stenosis. *Atherosclerosis*. 2011;219:694–697.

60. Su Y, Swift M. Mortality rates among carriers of ataxia-telangiectasia mutant alleles. *Ann Intern Med*. 2000;133:770–778.

61. Qi Y, Feng W, Song A, Song H, Yan S, Sun Q, Yang P. Role of serum IL-23/IL-17 axis in the relationship between periodontitis and coronary heart disease. *Int J Periodontics Restorative Dent*. 2013;33:185–191.

Novelty and Significance

What Is Known?

- Granulocyte macrophage colony-stimulating factor (GM-CSF) is a growth factor for myeloid cells and can also induce myeloid cells to produce the cytokine interleukin (IL)-23.
- In the setting of early atherosclerosis in mice, GM-CSF deficiency surprisingly has only a modest effect on total lesional cellularity and lesion area.

What New Information Does This Article Contribute?

- Deficiency of GM-CSF in the setting of advanced atherosclerosis in mice decreases the expression of IL-23 by lesional myeloid cells and suppresses both advanced lesional myeloid cell apoptosis and plaque necrosis, indicating associations among GM-CSF, IL-23, and apoptosis in atherosclerosis.
- The protective effect of GM-CSF deficiency in advanced plaque progression is abrogated by administration of IL-23, suggesting that IL-23 links GM-CSF to lesional myeloid cell apoptosis.

- IL-23 enhances the sensitivity of cultured macrophages and dendritic cells to apoptosis by downregulating the antiapoptotic protein Bcl-2 and by increasing oxidative stress, and advanced lesions of GM-CSF–deficient atherosclerosis-prone mice have lower levels of Bcl2 and increased oxidative stress.

The types of atherosclerotic plaques that cause acute cardiovascular events in humans are characterized by prominent areas of lesional cell apoptosis, but the mechanisms remain to be fully explored. Our current study reveals a new apoptosis pathway in which an endogenous molecule in lesions, GM-CSF, induces IL-23 in lesional myeloid cells, which then enhances the sensitivity of these cells to apoptosis. IL-23 enhances apoptosis by downregulating the antiapoptotic protein Bcl-2 and by increasing oxidative stress. In view of the implementation of anti–IL-23 therapy for other disorders, its focused use in high-cardiovascular risk subjects may provide a novel means to delay the formation of vulnerable plaques.

Subramanian *et al.*

Identification of a non-growth factor role for GM-CSF in advanced atherosclerosis: promotion of macrophage apoptosis and plaque necrosis through IL-23 signaling

Detailed Methods

Immunohistochemistry

Frozen aortic root sections were fixed using cold acetone followed by 3 washes with 1X PBS. The sections were blocked using Dako Protein block followed by incubation with primary antibody for 3 h at room temperature or for 16 h at 4°C. The sections were then washed with PBS and incubated with appropriate fluorochrome-conjugated secondary antibody for 1 h at room temperature. Nuclei were counterstained using either DAPI or Hoechst. Fluorescence microscopic images were acquired using a Olympus IX-70 microscope and images were analyzed using ImageJ. Primary antibodies against CD11c, CD3, Ly6G, CD45, and CD115 were obtained from BD biosciences. Antibodies against Bcl-2, phospho-serine, MKP-1, and p47(phox) were purchased from Santa Cruz Biotechnology. Antibodies against cleaved caspase-3, ubiquitin, pERK1/2, total ERK1/2, pMEK, total MEK, and β-actin were purchased from Cell Signaling Technology.

Laser capture microdissection and RT-PCR

RNA was captured from the intimal region of aortic root sections using a PALM laser capture microdissection (LCM) machine. The RNA, which was captured in RNA lysis buffer, was isolated using the RNAqueous Micro kit (Ambion) followed by RNA amplification using the MessageAmpII aRNA kit (Ambion). The amplified RNA was converted to cDNA using SuperScript VILO cDNA synthesis kit (Invitrogen). RT-PCR was conducted on a 7500 Realtime PCR system (Applied Biosystems) using SYBR green chemistry following standard curve method. The sequences of primers used in this study are: IL-12 p40 (5′-CCTGCATCTAGAGGCTGTCC-3′ / 5′-GGCAAACCAGGAGATGGTTA-3′); TNF-α (5′-CATCTTCTCAAAATTCGAGTGACAA-3′ / 5′-TGGGAGTAGACAAGGTACAACCC-3′); IFN-γ (5′-GCGTCATTGAATCACACCTG-3′ / 5′-TGAGCTCATTGAATGCTTGG-3′); IL-10 (5′-CATGGGTCTTGGGAAGAGAA-3′ / 5′-AACTGGCCACAGTTTTCAGG-3′); TGF-β (5′-GGACTCTCCACCTGCAAGAC-3′ / 5′-GACTGGCGAGCCTTAGTTTG-3′); IL-2 (5′-AAGCTCTACAGCGGAAGCAC-3′ / 5′-ATCCTGGGGAGTTTCAGGTT-3′); GATA3 (5′-GTCATCCCTGAGCCACATCT-3′ / 5′-AGGGCTCTGCCTCTCTAACC-3′); Tbet (5′-GGTGTCTGGGAAGCTGAGAG-3′ / 5′-GAAGGACAGGAATGGGAACA-3′); FoxP3 (5′-TCTTGCCAAGCTGGAAGACT-3′ / 5′-GGGGTTCAAGGAAGAAGAGG-3′); IL-17A (5′-TCTCTGATGCTGTTGCTGCT-3′ / 5′-AGGAAGTCCTTGGCCTCAGT-3′); RORγT (5′-AAGCTGAAGGCAGAGACAGC-3′ / 5′-TGTTCTGGTTCCCCAAGTTC-3′). Primers against Bcl-2, IL-23 p19 and IL-6 were purchased from Qiagen.

IL-23 ELISA

IL-23 levels in serum were quantified by ELISA using a commercially available kit (Mouse IL-23 (second generation) ELISA Ready-SET GO, Ebiosciences) following the manufacturer's protocol. For measurement of IL-23 levels in atherosclerotic lesions, lesional extracts were obtained by treating 6 aortic root sections from each mouse with a buffer containing 0.5% Triton X-100, 150 mM NaCl, 15 mM Tris, 1 mM CaCl2, and 1 mM $MgCl_2$, pH 7.4. ELISA for IL-23 was conducted on these lesional extracts.

Bone-marrow derived macrophage (BMDM) culture
Bone-marrow cells were isolated from WT C57BL/6J mice and cultured in DMEM supplemented with 10% FBS and 10% L-cell conditioned medium as described previously. The cells were cultured for 7 days, with fresh medium being replenished on day 3 of culture.

Plasmid transfection and Immunoprecipitation
Bone marrow-derived macrophages were transfected with pSFFV-neo-Bcl-2 cDNA (Addgene plasmid 8750) using jetPEI-macrophage transfection reagent using the manufacturer's protocol. Experiments were conducted 48 h post-transfection. Bcl-2-overexpresing cells were treated without or with IL-23 (10 ng/ml) in the presence of proteasomal inhibitor MG-132 (10 µM) followed by lysis in a buffer (IP buffer) containing 20 mM Tris-HCl (pH 7.5), 150 mM NaCl, 1 mM $MgCl_2$, 1 mM $CaCl_2$, 1% Triton X-100, and 1 tablet of Roche EDTA-free protease inhibitor per 10 ml of buffer. The lysates were then incubated with anti-Bcl-2 antibody and Protein G sepharose beads (Cell Signaling Technology) at 4°C for 16 h on a rotator-shaker. The samples were washed 3X with IP buffer followed by addition of Laemmli buffer and boiling. These samples were then used for Western blotting.

Western blotting from lesional extracts
Protein extracts from atherosclerotic lesional material was obtained by addition of Laemmli buffer directly on top of 6 aortic root sections (8 µm thickness) from each mouse. The samples were additionally denatured by boiling and then subjected to SDS-PAGE and Western blotting using standard techniques.

Assay of lesional ROS and fibrous cap thickness
Frozen aortic root sections were incubated with 10 µM DHE for 30 min at room temperature. Following 3 washes with 1X PBS, the slides were mounted and immediately analyzed by fluorescence microscopy. ROS was quantified by measurement of mean fluorescence intensity (MFI) using ImageJ software. To assay fibrous cap thickness, aortic root sections were stained with picrosirius red, and microscopic images were quantified for fibrous cap thickness-to-lesion area using image processing.

Assay of ROS in cultured cells
Macrophages were incubated with CellROX (5 µM) for 20 min at 37°C. ROS was quantified by measurement of MFI as determined by flow-cytometry using a FACS Canto-II (Becton Dickinson) flow-cytometer.

Supplementary Figure Legends

Online Figure I. GM-CSF is absent in the lesions of *Csf2$^{-/-}$Ldlr$^{-/-}$* mice. Immunofluorescence microscopy of aortic root sections from 12-wk WD-fed *Ldlr$^{-/-}$* and *Csf2$^{-/-}$Ldlr$^{-/-}$* mice immunostained with anti-GM-CSF antibody (green). DAPI was used to label the nuclei (blue). Bar, 50 μm.

Online Figure II. GM-CSF is produced by lesional macrophages, DCs, and smooth muscle cells. Aortic root sections from 12-wk WD-fed *Ldlr$^{-/-}$* mice were immunostained with an anti-GM-CSF antibody (red) and either anti-CD11c (DCs), anti-F4/80 (macrophages), or anti-sm-α-actin (smooth muscle cells) (green) antibodies. The regions of co-localization appear yellow in the merged image. Bar, 5 μm.

Online Figure III. Lesional DC and T cell numbers are lower in *Csf2$^{-/-}$Ldlr$^{-/-}$* mice. A, Total cell number per lesional section was calculated by microscopic analysis of DAPI-stained sections using ImageJ. **B,** Quantification of number of macrophages (CD11c^{lo}F4/80^{+}), DCs (CD11c^{hi}MHC-II^{hi}), smooth muscle cells (SMC, sm-actin+), T cells (CD3^{+}), and neutrophils (Ly6G^{+}) in the atherosclerotic lesions of 12-wk WD-fed *Ldlr$^{-/-}$* and *Csf2$^{-/-}$Ldlr$^{-/-}$* mice. **C,** Flow-cytometric quantification of monocytes and neutrophils in the peripheral blood of 12 wk WD-fed *Ldlr$^{-/-}$* and *Csf2$^{-/-}$Ldlr$^{-/-}$* mice; the data are expressed as percent of total leukocytes. For A and B, n=10 mice per group; *, p<0.05 *vs. Ldlr$^{-/-}$* mice; n.s., no significant difference.

Online Figure IV. *Csf2$^{-/-}$Ldlr$^{-/-}$* mice have decreased cleaved caspase-3+ lesional cells. Aortic root sections of 12-wk WD-fed *Ldlr$^{-/-}$* and *Csf2$^{-/-}$Ldlr$^{-/-}$* mice were immunostained with an antibody recognizing the active cleaved form of caspase-3 (green). DAPI was used to stain the nuclei (blue). Bar, 25 μm.

Online Figure V. *Csf2$^{-/-}$Ldlr$^{-/-}$* mice have decreased lesional apoptotic macrophages and DCs. Percent lesional cells that were either apoptotic macrophages, DCs, or smooth muscle cells (SMC) as assessed by microscopic analysis of atherosclerotic lesional sections of 12-wk WD-fed *Ldlr$^{-/-}$* and *Csf2$^{-/-}$Ldlr$^{-/-}$* mice. The sections were double labeled with TUNEL to detect apoptotic cells and either anti-CD11c (DCs), anti-F4/80 (macrophages), or anti-sm-α-actin (SMCs). n=10 mice per group; *, p<0.05 *vs. Ldlr$^{-/-}$* mice.

Online Figure VI. Fibrous cap thickness and intimal elastin are unaffected in *Csf2$^{-/-}$Ldlr$^{-/-}$* mice. A, Atherosclerotic lesions of 12-wk WD-fed *Ldlr$^{-/-}$* and *Csf2$^{-/-}$Ldlr$^{-/-}$* mice were stained with picosirius red, and the mean collagen cap thickness was measured. **B,** Intimal elastin content was measured as a percentage of total lesion area that stained positive for Verhoeff-Van Gieson dye. n = 10 mice per group; n.s., no significant difference.

Online Figure VII. Splenic and peripheral blood T cell numbers are unaffected in *Csf2$^{-/-}$Ldlr$^{-/-}$* mice. A, RT-PCR analysis of expression levels of indicated genes in RNA isolated from the spleens of 12-wk WD-fed *Ldlr$^{-/-}$* and *Csf2$^{-/-}$Ldlr$^{-/-}$* mice. All data are normalized to *Actb* mRNA. **B-D,** Flow-cytometric quantification of total number of splenic T cells, CD4+ and CD8+ T cells, and Tregs in 12-wk WD-fed *Ldlr$^{-/-}$* and *Csf2$^{-/-}$Ldlr$^{-/-}$* mice. **E,** Flow-cytometric quantification of total T cells, CD4+, and CD8+ T cells in the peripheral blood of 12-wk WD-fed *Ldlr$^{-/-}$* and *Csf2$^{-/-}$Ldlr$^{-/-}$* mice. n = 5 mice per group. *, p < 0.05 *vs. Ldlr$^{-/-}$* mice; n.s., no significant difference.

Online Figure VIII. Serum IL-23 levels are not lower in *Csf2^{-/-}Ldlr^{-/-}* mice. Serum IL-23 levels in 12-wk WD-fed *Ldlr^{-/-}* and *Csf2^{-/-}Ldlr^{-/-}* mice, as measured by ELISA. n=10 mice per group; n.s., no significant difference.

Online Figure IX. Lesional macrophages and DCs produce IL-23. Aortic root sections from 12-wk WD-fed *Ldlr^{-/-}* mice were immunostained with anti-IL23 Ab and either anti-CD11c (DCs), anti-F4/80 (macrophages), or anti-sm-α-actin (SMCs) and viewed by fluorescence microscopy. Nuclei were labeled with DAPI (blue). Bar, 25 µm.

Online Figure X. *Csf2^{-/-}Ldlr^{-/-}* mice have lower expression of IL-23 in lesional macrophages and DCs. Immunofluorescence quantification (mean fluorescence intensity, MFI) of IL-23 in F4/80+ macrophage-rich and CD11c+ DC-rich regions of aortic root atherosclerotic lesions in 12-wk WD-fed *Ldlr^{-/-}* and *Csf2^{-/-}Ldlr^{-/-}* mice. n = 10 mice per group; *, $p < 0.05$ vs. *Ldlr^{-/-}* mice.

Online Figure XI. IL-23 enhances 7KC-induced apoptotic susceptibility in macrophages. Representative images of annexin-V labeling (red) in cultured macrophages treated with vehicle (control) or 7KC (35 µM) for 18 h in the presence or absence of indicated concentrations of IL-23. Bar, 5 µm.

Online Figure XII. IL-23 enhances apoptosis susceptibility in macrophages to other atherosclerosis-relevant stimuli. Microscopic analysis and quantification of percent macrophages that label positive for annexin-V following exposure to oxidized-LDL (OxLDL, left panel) or a combination of thapsigargin and KOdiA-PC (right panel) for 24 h in the presence or absence of IL-23. The data are representative of two independent experiments. *, $p < 0.05$ *vs.* control; #, $p < 0.05$ *vs.* OxLDL-treated group.

Online Figure XIII. TNF, IFN-γ, IL-2, and IL-6 do not enhance apoptosis susceptibility in macrophages. Microscopic analysis and quantification of percent macrophages that label positive for annexin-V following exposure to 7KC for 16 h in the presence or absence of indicated concentrations of TNF-α, IL-2, IFN-γ, or IL-6. *, $p < 0.05$ *vs.* control; n.s., no significant difference.

Online Figure XIV. IL-23 enhances 7KC-induced apoptosis of DCs. Microscopic analysis and quantification of percent bone marrow-derived DCs that label positive for annexin-V following exposure to 7KC for 16 h in the presence or absence IL-23 (10 ng/ml).

Online Figure XV. Cytokine mRNA analysis of aortic root lesions *Csf2^{-/-}Ldlr^{-/-}* mice treated with IL23.   RNA was obtained by LCM from atherosclerotic lesions of 12 wk WD-fed *Ldlr^{-/-}* (left panel) and *Csf2^{-/-}Ldlr^{-/-}* mice (right panel) treated with saline (Veh) or rIL-23 (5 µg/kg). The captured RNA was then analyzed for the indicated cytokine mRNAs by RT-QPCR. n = 3 mice for vehicle treated group and n = 6 mice for rIL-23-treated group; *, $p < 0.05$ *vs.* Veh; n.s., no significant difference.

Online Figure XVI. IL-17 neutralizing antibody is functional *in vivo*. Analysis of *Il6* expression by RT-PCR of RNA extracted from atherosclerotic lesions of WD-fed *Ldlr^{-/-}* mice treated with control IgG or anti-IL17 Ab, and *Csf2^{-/-}Ldlr^{-/-}* mice treated with IL-23 plus control IgG or anti-IL17 Ab as indicated. n=3 mice per group; *, $p<0.05$ *vs.* IgG treated *Ldlr^{-/-}* mice; #, $p<0.05$ *vs.* IL23 and IgG treated *Csf2^{-/-}Ldlr^{-/-}* mice.

Online Figure XVII. IL-23 enhances 7KC-induced activation of pro-caspase9. A, Immunoblot analysis of pro-caspase9 in macrophages treated with vehicle (Con), 7KC alone, IL23 alone, or the combination of 7KC and IL23 for 16 h. β-actin was used as loading control. **B,** BMDM obtained from *Caspase9^{fl/fl}* mice were transduced with adenovirus expressing LacZ (Ad-LacZ) or Cre recombinase (Ad-Cre) at an MOI of 1:500. Caspase 9 knockdown in the Ad-Cre group was confirmed by immunoblot analysis at 48 h post-transduction. The macrophages were treated with 7KC alone, IL-23 alone, or the combination of 7-KC and IL-23 for 18 h. Apoptosis was quantified by microscopic analysis of Annexin-V labeled cells. *, p<0.05 *vs.* control; #, p<0.05 *vs.* 7-KC treatment; n.s. no significant difference. The data are representative of 2 independent experiments.

Online Figure XVIII. IL-23 does not affect *Bcl2* mRNA expression. A, Immunoblot of Bcl-2 in bone marrow-derived DCs treated with vehicle (Con) or 7KC (35 µM) for 8 h in the presence or absence of IL-23 (10 ng/ml). β-actin was used as loading control. Analysis of *Bcl2* mRNA expression relative to *Actb* in macrophages treated with IL-23 (10 ng/ml) for 4, 8, or 16 h. The data are representative of 2 independent experiments. *, p , 0.05 *vs.* control; n.s., no significant difference.

Online Figure XIX. Inhibition of ERK activity decreases Bcl-2 protein levels. A, Immunoblot of Bcl-2 in macrophages treated with vehicle (con) or ERK inhibitor PD98059 (1 µM) for 6 h. β-actin was used as loading control. **B,** Immunoblot of phospho- and total MEK in macrophages treated with IL-23 alone or the combination of 7KC plus IL-23 for 30 min.

Online Figure XX. Lesional MKP-1 expression is lower in *Csf2^{-/-}Ldlr^{-/-}* mice. A, Immunofluorescence of MKP-1 (red) in aortic atherosclerotic lesions of *Ldlr^{-/-}* and *Csf2^{-/-}Ldlr^{-/-}* mice. Nuclei were labeled with Hoechst dye (blue). Bar, 10 µm. **B,** Immunofluorescence of MKP-1 in macrophages transfected with negative control siRNA (siNC) or *Mkp1* siRNA (siMKP1). Bar, 5 µm. **C,** Immunoblot of MKP-1 in atherosclerotic lesional extracts of 12-wk WD-fed *Ldlr^{-/-}* and *Csf2^{-/-}Ldlr^{-/-}* mice. n=6 mice per group. β-actin was used as the loading control. The bar graph represents the densitometric ratio quantification of the immunoblot data. *, p<0.05 *vs. Ldlr^{-/-}* mice. MFI, mean fluorescence intensity.

Online Figure XXI. Lesional Bcl-2 expression is higher in *Csf2^{-/-}Ldlr^{-/-}* mice. Representative images of Bcl-2 immunofluorescence (green) in aortic root atherosclerotic lesions of 12-wk WD-fed *Ldlr^{-/-}* and *Csf2^{-/-}Ldlr^{-/-}* mice. Nuclei were labeled with Hoechst (blue). Bar, 25 µm.

Online Figure XXII. Bcl-2 is higher in the lesions of *Csf2^{-/-}Ldlr^{-/-}* mice and is decreased upon IL-23 restoration. Representative images of fluorescence microscopic analysis and quantification of Bcl-2 expression by immunostaining in aortic atherosclerotic lesions of 12-wk WD-fed *Ldlr^{-/-}* and *Csf2^{-/-}Ldlr^{-/-}* mice treated with saline (Veh) or rIL-23 (5 µg/kg). Bar, 25 µm.

Online Figure XXIII. IL-23-induced Bcl-2 degradation enhances 7KC-induced ROS. A, **B, and D,** Representative flow-cytometry histograms of CellROX staining as a measure of ROS generation in macrophages subjected to the indicated treatments. **C,** Immunoblot of Bcl-2 in macrophages transfected with negative control siRNA (siNC) or *Bcl2* siRNA (siBcl2) and then treated without or with IL23 for 8 h. The bar graph shows the densitometric ratio analysis of the immunoblot data. β-actin was used as a loading control. *, p < 0.05 *vs.* siNC; n.s., no significant difference.

Online Figure XXIV. A, Representative images of DHE-stained lesions (red) as a measure of lesional ROS in aortic atherosclerotic lesions of 12-wk WD-fed *Ldlr^{-/-}* and *Csf2^{-/-}Ldlr^{-/-}* mice. **B,**

Similar to **A**, but the mice were administered either saline (Veh) or rIL-23. The broken white line demarcates the intima of the atherosclerotic lesion. Bar, 25 μm.

Supplementary Table and Figures

		Body Weight (g)	Cholesterol (mg/dl)	Triglycerides (mg/dl)	Glucose (mg/dl)	Insulin (ng/ml)
Male	*Ldlr-/-* (12)	37.2±2.8	716.5±34.1	538.4±31.2	157.4±18.2	0.67±.1
	Csf2-/-Ldlr-/- (14)	35.6±2.4	686.2±40.5	600±41.5	166±28.9	.63±.15
Female	*Ldlr-/-* (13)	27.6±1.9	674.8±23.6	410.5±28.6	140.3±10.8	.49±.09
	Csf2-/-Ldlr-/- (17)	27.1±1.7	700.4±17.2	394.6±38.2	141.5±12.4	.52±.11

Online Table I. Measurement of body weight, plasma cholesterol, triglycerides, glucose, and insulin in 12-wk WD-fed male and female *Ldlr*^{-/-} and *Csf2*^{-/-}*Ldlr*^{-/-} mice. The number in the bracket indicates the number of mice in each group.

Online Figure I

DAPI | GM-CSF | Merge — *Ldlr⁻ᐟ⁻*

DAPI | GM-CSF | Merge — *Csf2⁻ᐟ⁻ Ldlr⁻ᐟ⁻*

Online Figure II

CD11c | GM-CSF | Merge

F4/80 | GM-CSF | Merge

Sm-actin | GM-CSF | Merge

Online Figure III

A

B

C
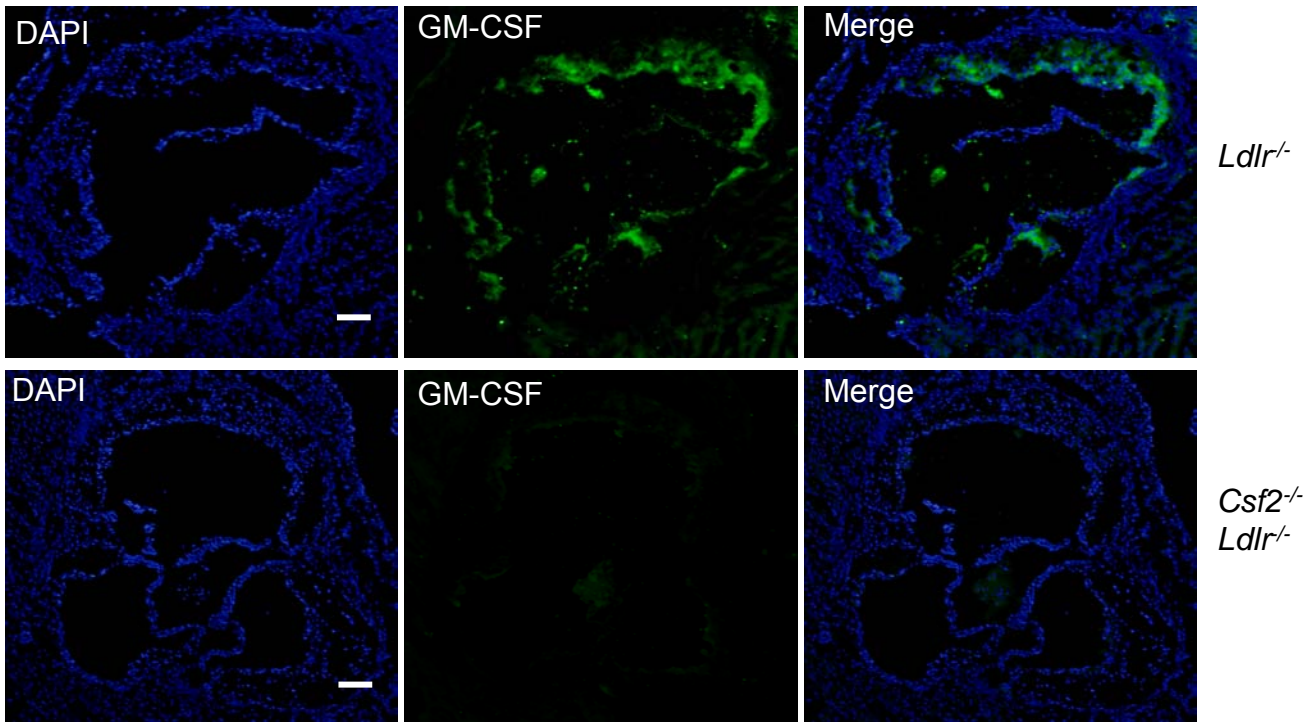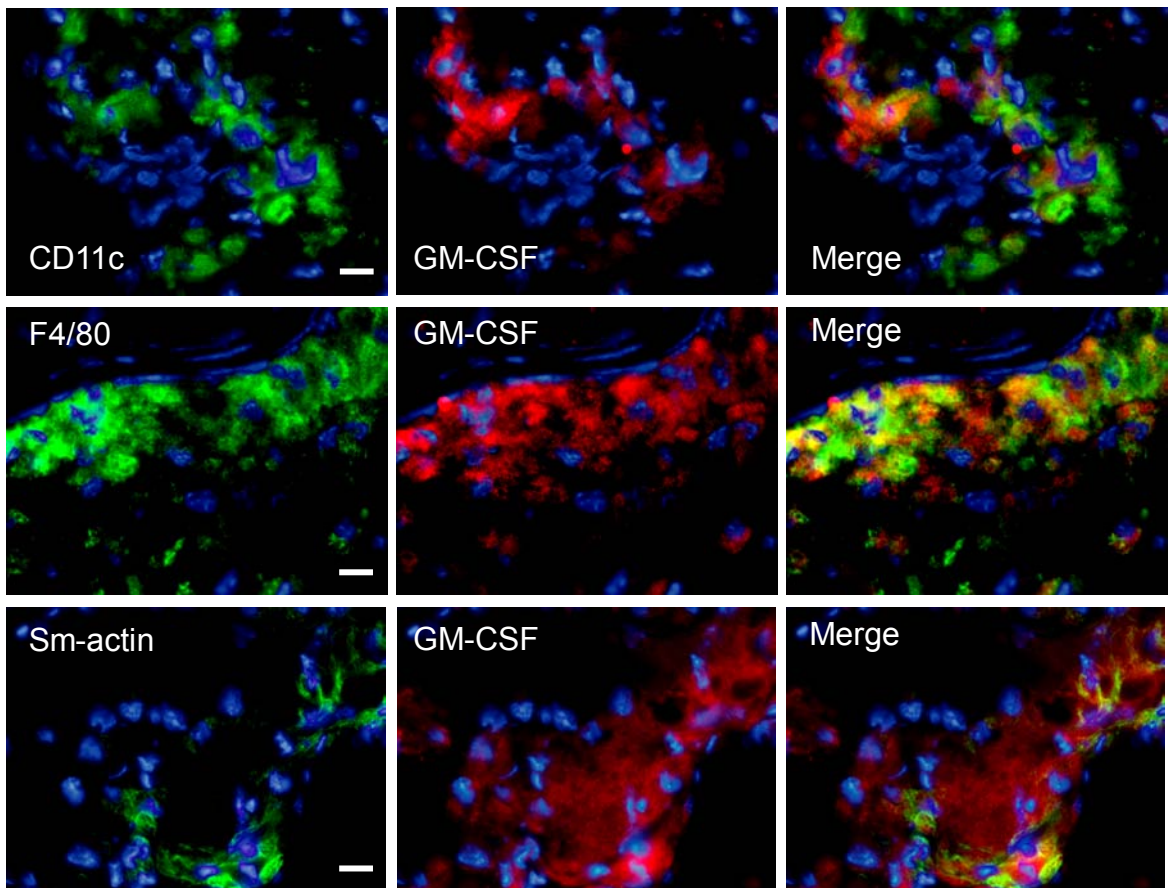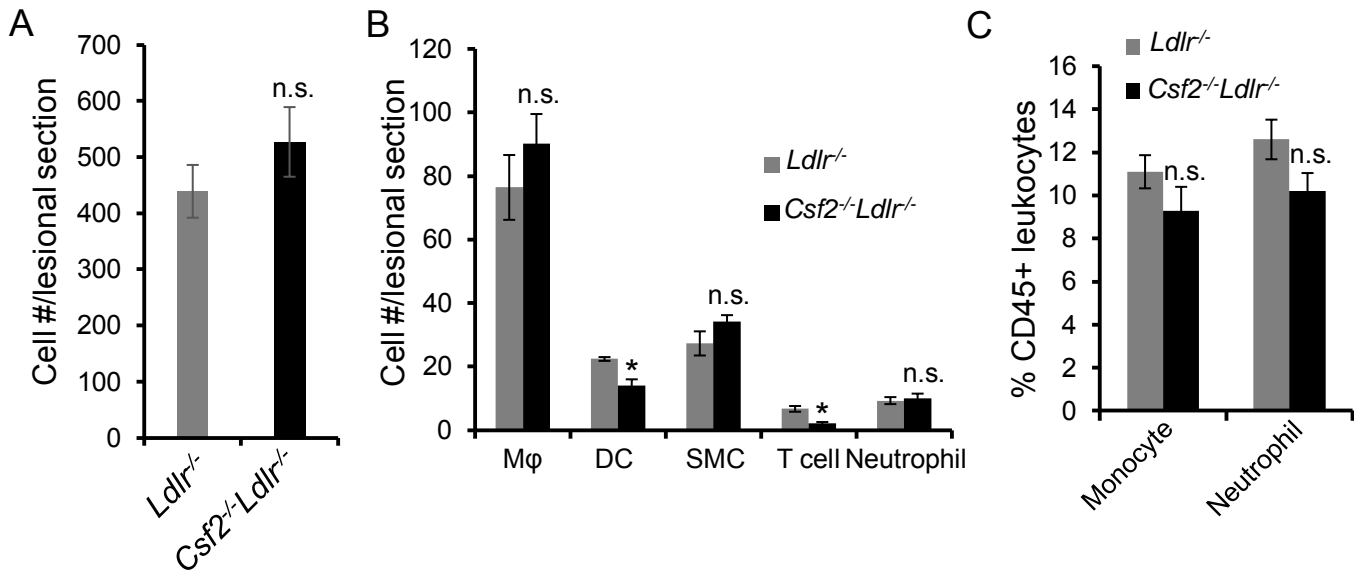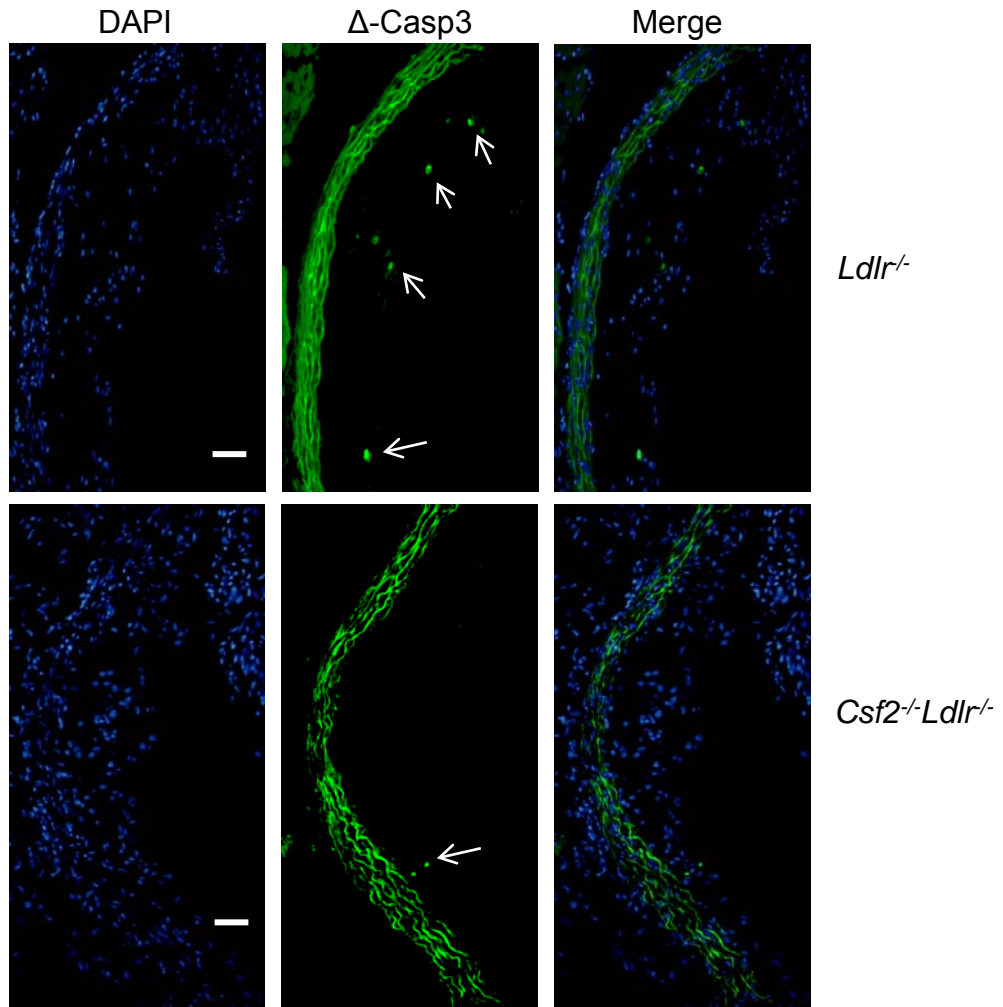
Online Figure IV

Online Figure V
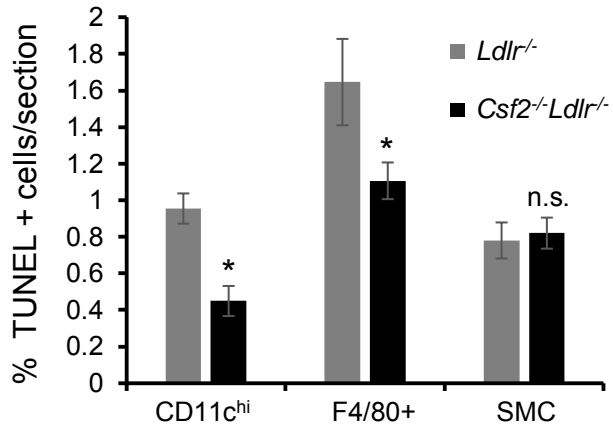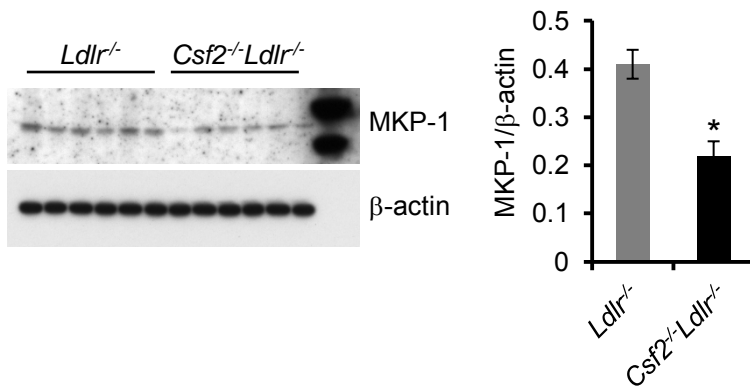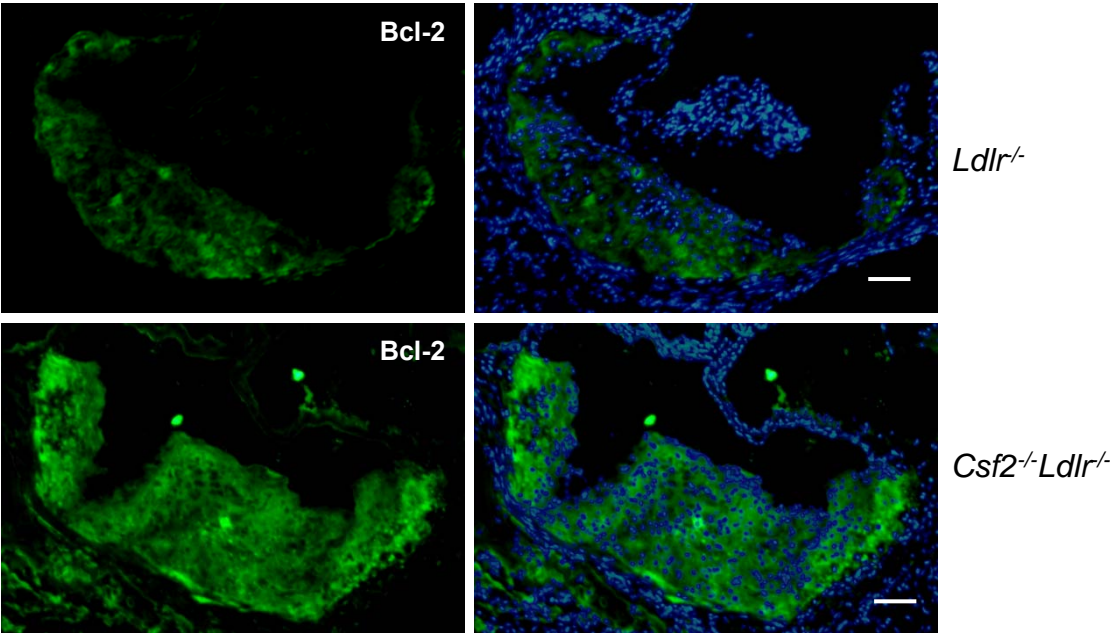

Online Figure VI
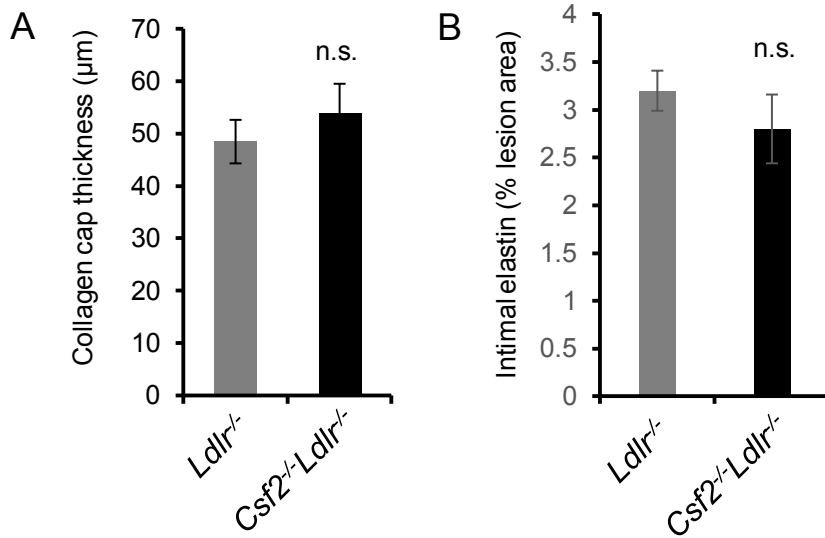
Online Figure VII

A
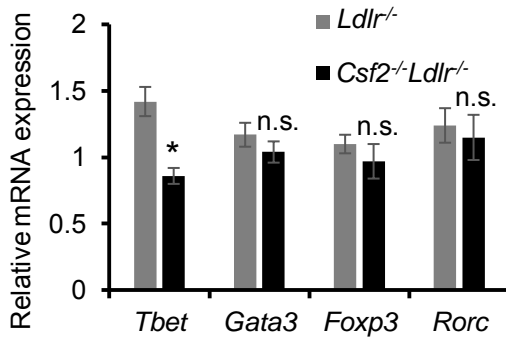
B
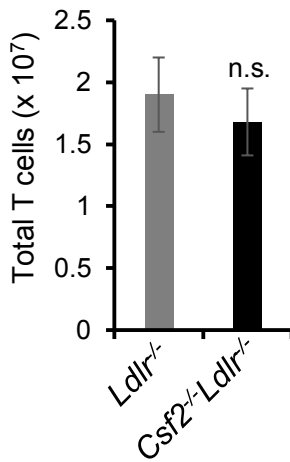
C
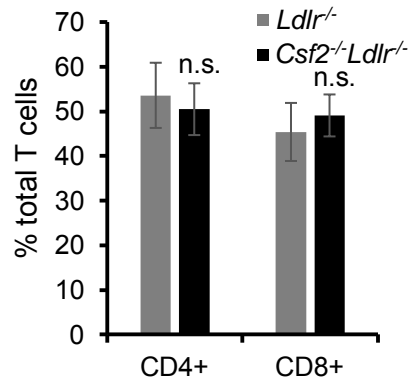
D

E
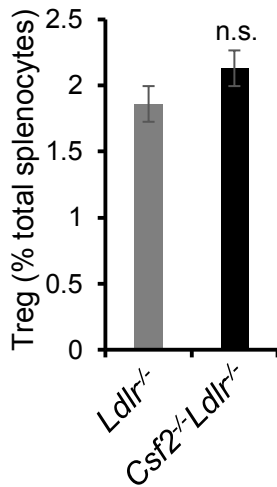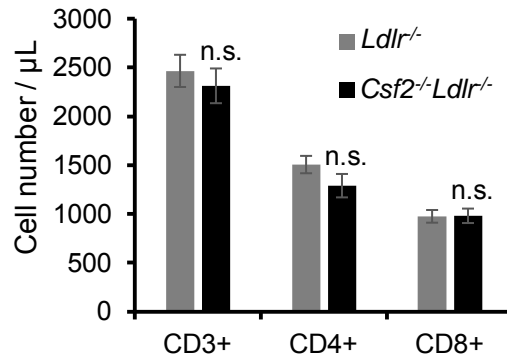
Online Figure VIII
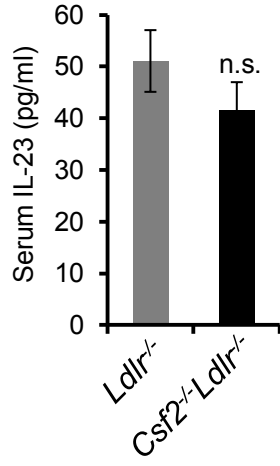
Online Figure IX
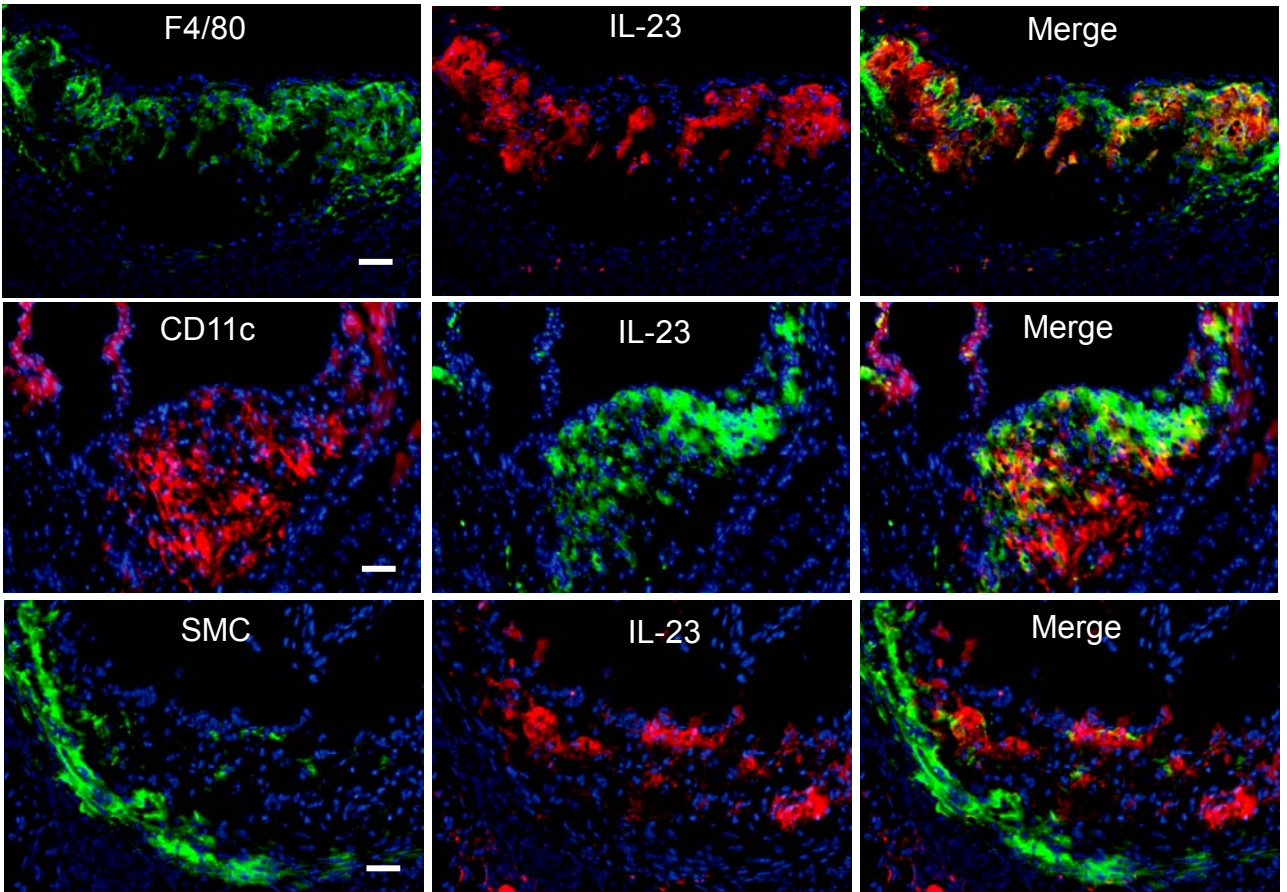
Online Figure X

Online Figure XI

Control

7KC

7KC + IL23- 10 ng/ml

7KC + IL23- 100 ng/ml
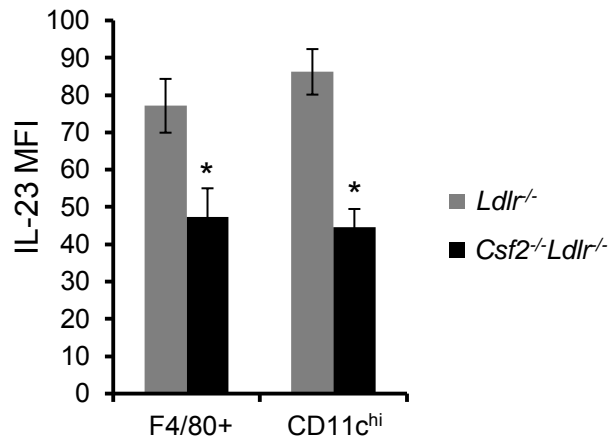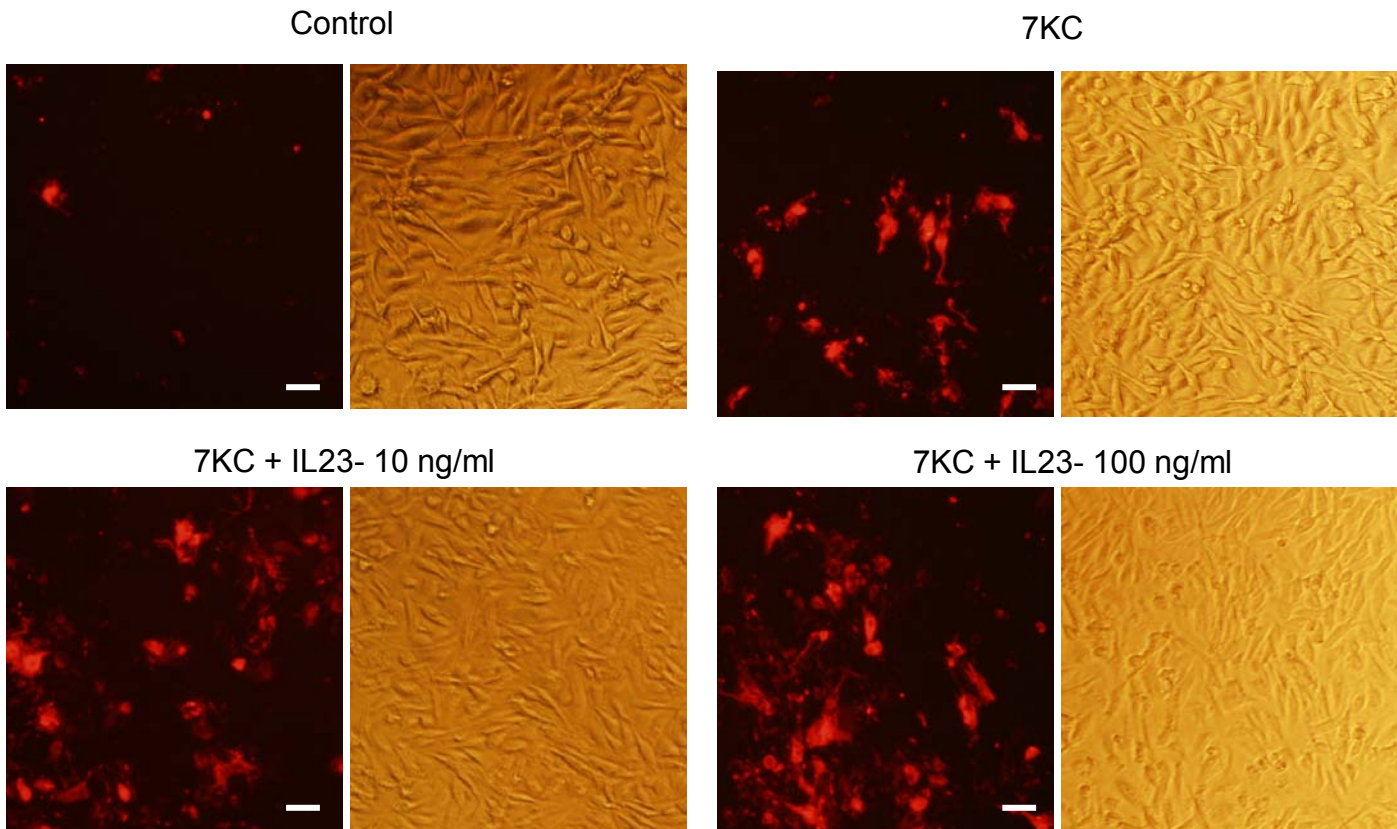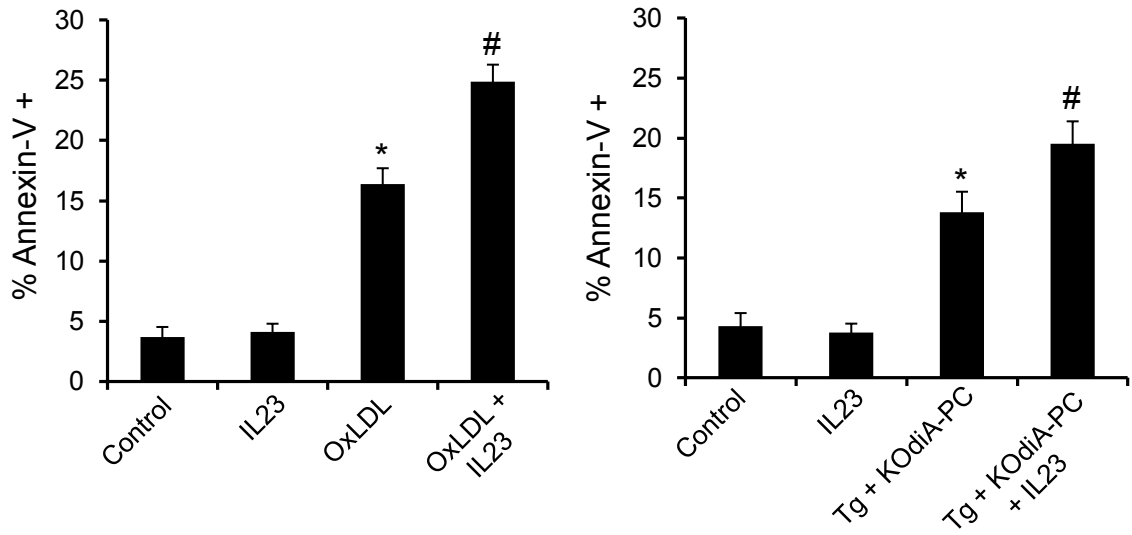
Online Figure XII

Online Figure XIII
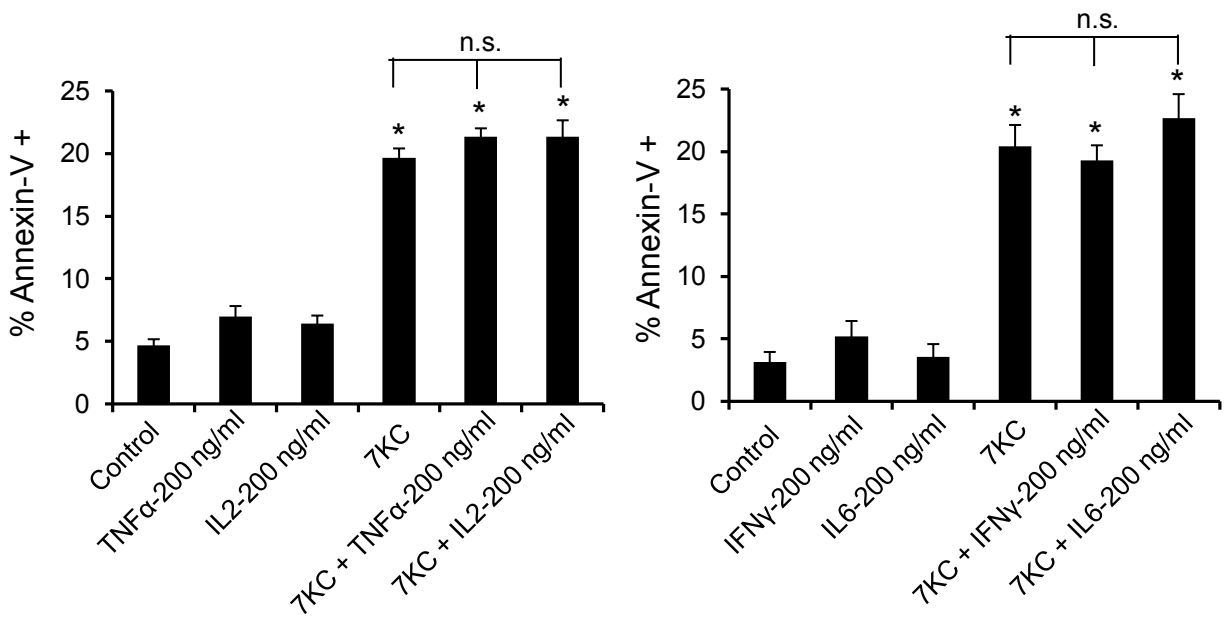
Online Figure XIV

Online Figure XV

$Ldlr^{-/-}$

$Csf2^{-/-}Ldlr^{-/-}$
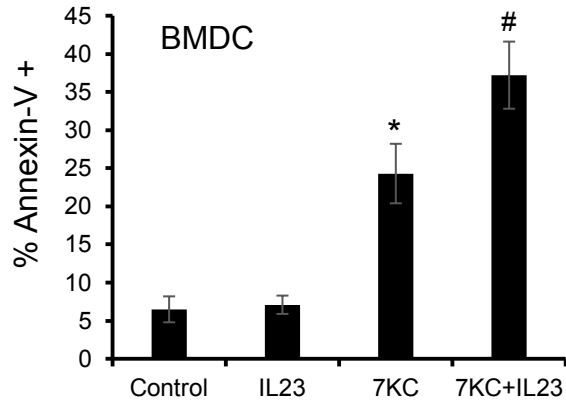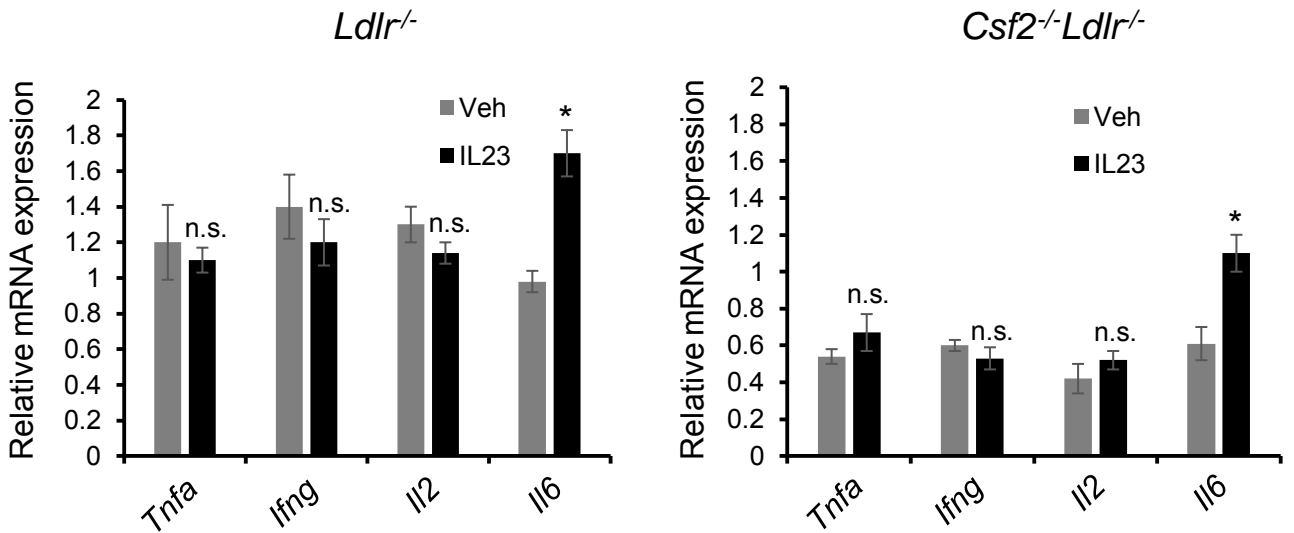
Online Figure XVI

Online Figure XVII
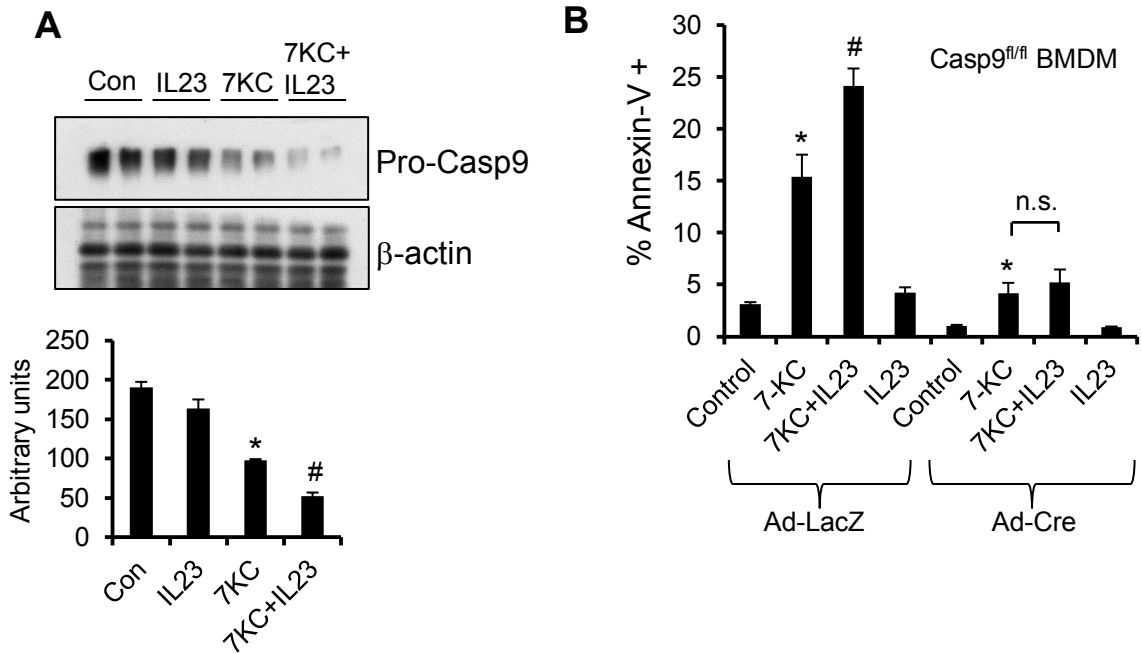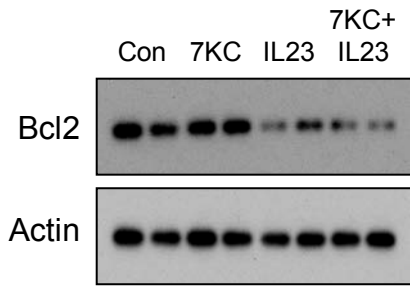
A

B

Online Figure XVIII
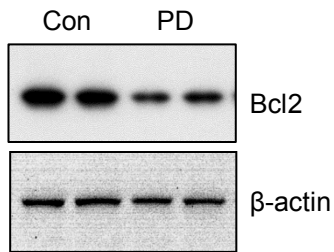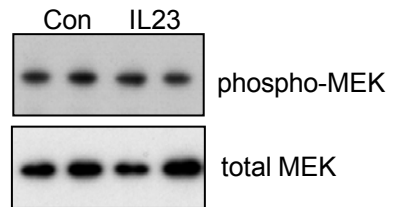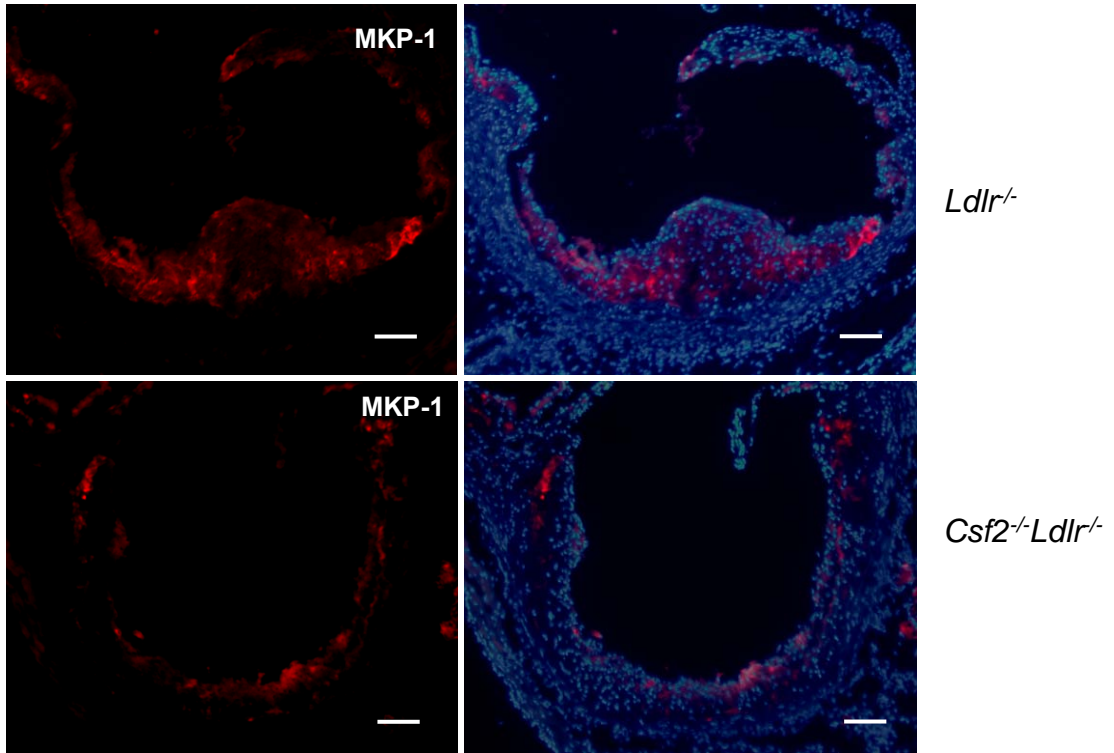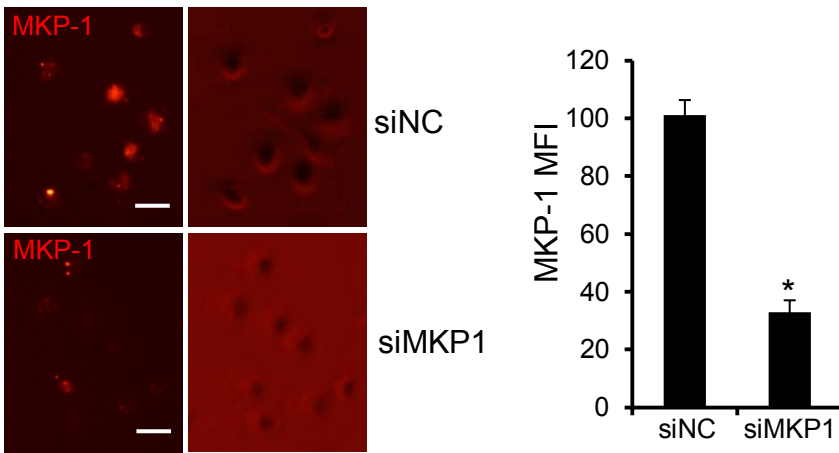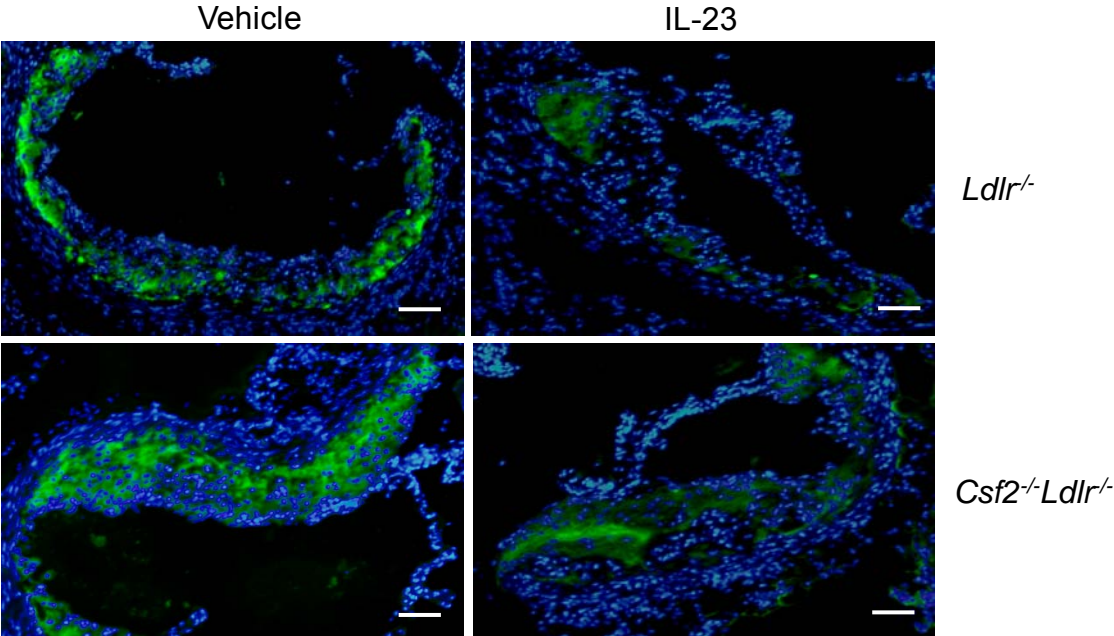
A

Bcl2

Actin

Con 7KC IL23 7KC+IL23

B

Relative *Bcl2* mRNA expression

n.s. n.s. n.s.

0 4 8 16

IL-23 - Time (h)

Online Figure XIX

A

Con PD

Bcl2

β-actin

B

Con IL23

phospho-MEK

total MEK

Online Figure XX

A

MKP-1

MKP-1

Ldlr⁻ᐟ⁻

Csf2⁻ᐟ⁻Ldlr⁻ᐟ⁻

B

MKP-1

siNC

MKP-1

siMKP1

C

Ldlr⁻ᐟ⁻   *Csf2⁻ᐟ⁻Ldlr⁻ᐟ⁻*

MKP-1

β-actin

Online Figure XXI

Ldlr^{-/-}

Csf2^{-/-}*Ldlr*^{-/-}

Online Figure XXII

Ldlr^{-/-}

Csf2^{-/-}*Ldlr*^{-/-}

A

B

C

D

Online Figure XXIV

A

Ldlr⁻/⁻ *Csf2⁻/⁻Ldlr⁻/⁻*

B

Vehicle IL-23

Ldlr⁻/⁻

Csf2⁻/⁻Ldlr⁻/⁻
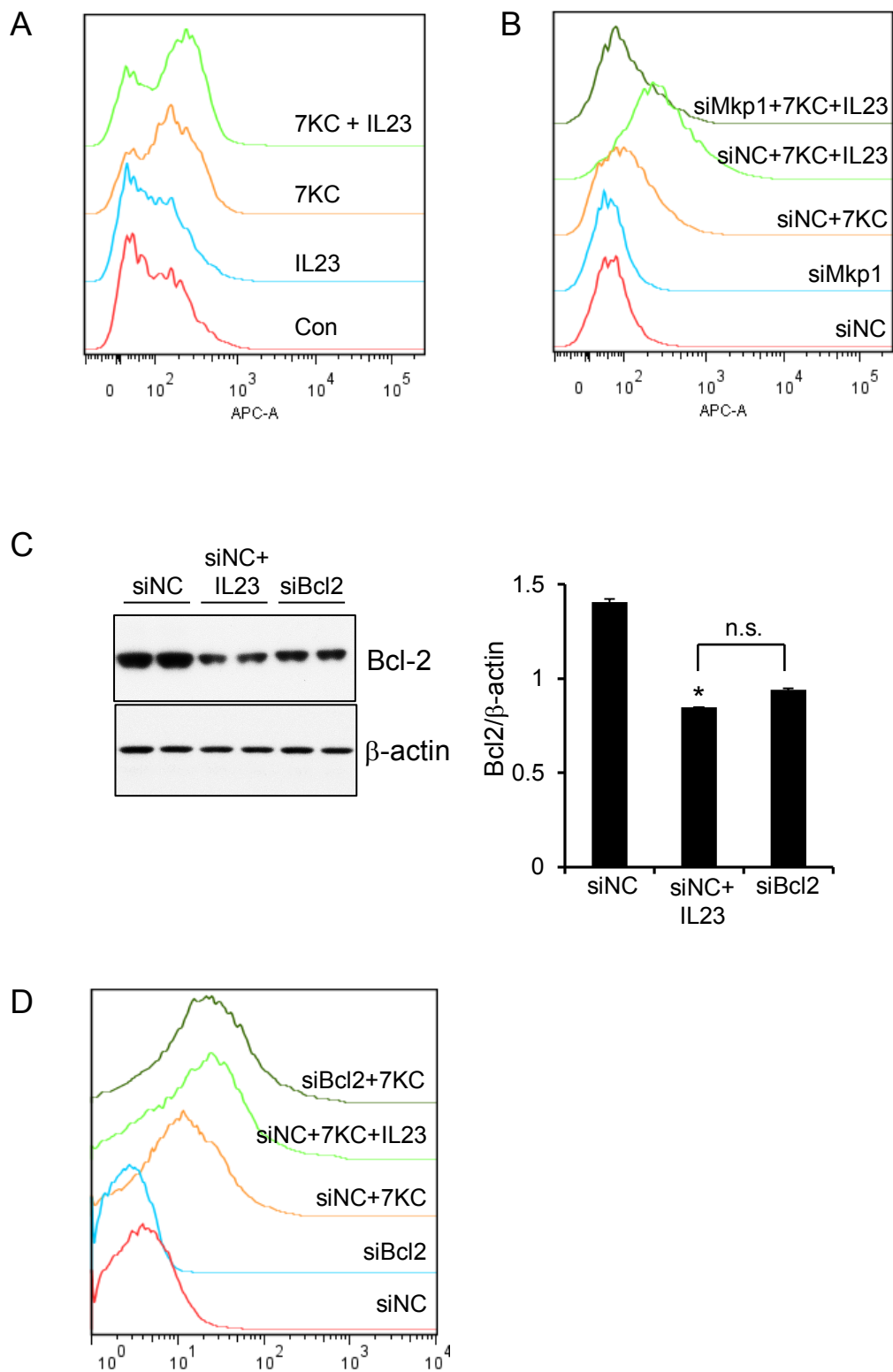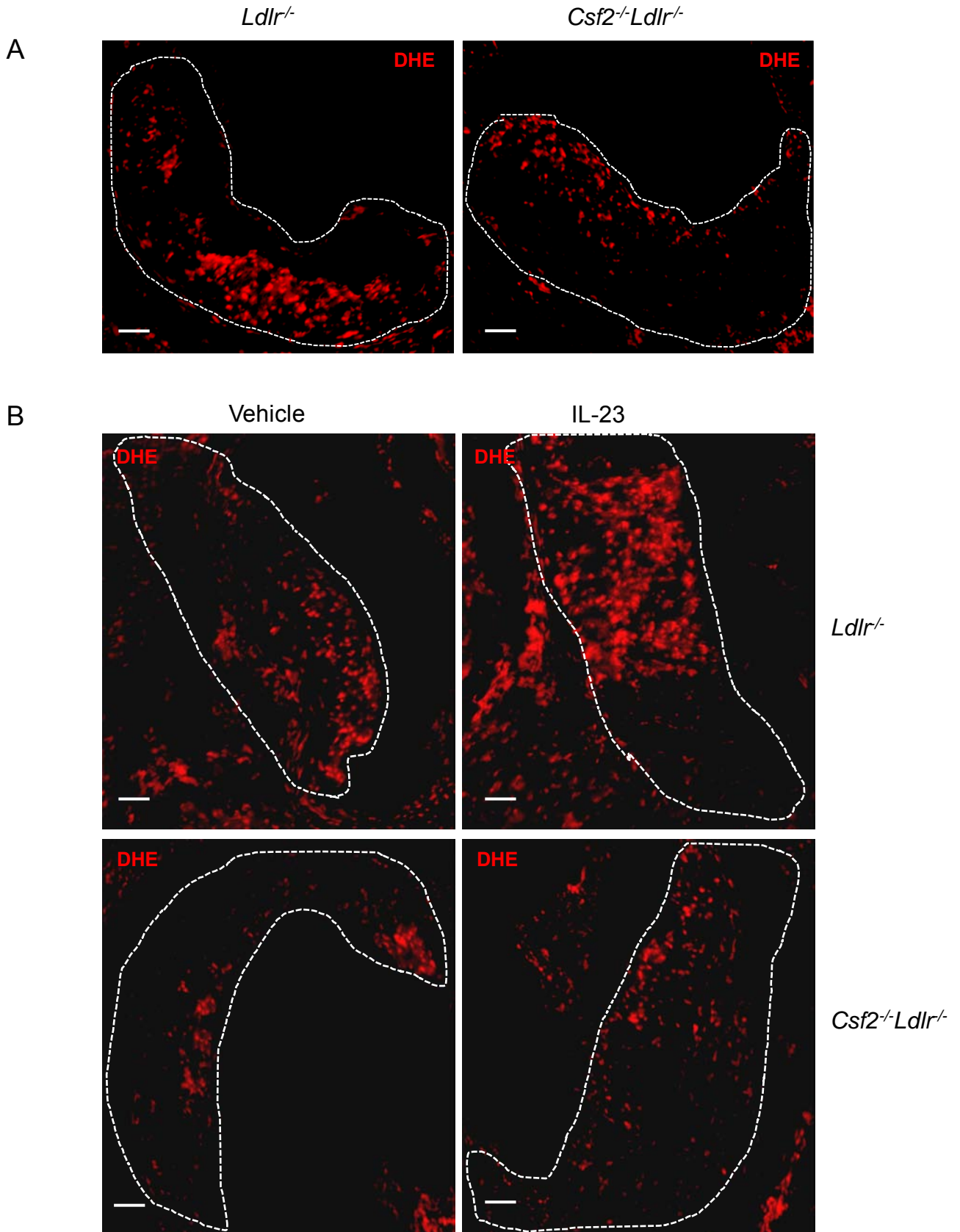
**Identification of a Non-Growth Factor Role for GM-CSF in Advanced Atherosclerosis:
Promotion of Macrophage Apoptosis and Plaque Necrosis Through IL-23 Signaling**
Manikandan Subramanian, Edward Thorp and Ira Tabas

The online version of this article, along with updated information and services, is located on the
World Wide Web at:
http://circres.ahajournals.org/content/116/2/e13

Data Supplement (unedited) at:
http://circres.ahajournals.org/content/suppl/2014/10/27/CIRCRESAHA.116.304794.DC1.html